In vitro ubiquitylation assay

RING-proline (RP)-HRD1-myc and Pael-R-FLAG were produced by T_NT quick-coupled transcription/translation systems (Promega). Sixteen microliters of T_NT reaction lysates producing RP-HRD1 or Pael-R-FLAG were mixed with other components including E1 (25 ng), E2 (GST-UbcH5c, 400 ng), and GST-ubiquitin (7 ng) in 100 μL of reaction buffer [40 mM Tris-HCl (pH 7.6), 5 mM $MgCl_2$, 2 mM ATP, and 2 mM dithiothreitol (DTT)]. The reaction mixtures were incubated at 30°C for 90 min, immunoprecipitated with anti-FLAG antibody, subjected to SDS-PAGE, and analyzed by western blotting using the anti-GST polyclonal antibody.

In vitro binding assay

RP-HRD1 was cloned into the pGEX 6p-1 vector (GE Healthcare Bio-Sciences). GST-RP-HRD1 and GST were expressed by culturing *Escherichia coli* DH5α with 0.5 mM isopropyl-β-D-thiogalactopyranoside (IPTG) for 4 h at 37°C. The cells were collected and lysed in a lysis buffer [10 mM HEPES (pH 7.4), 150 mM NaCl, 1 mM EGTA, 10%, 0.5% Triton X-100 with 1.5 mM phenylmethylsulfonyl fluoride (PMSF)]. The supernatants were mixed with glutathione-Sepharose 4B (GE Healthcare Bio-Sciences) for 16 h at 4°C. The beads were washed with lysis buffer and eluted with 50 mM Tris-HCl (pH 8.0) containing 10 mM reduced glutathione, and the eluted fraction dialyzed against PBS.

Equal amounts of purified GST or GST-RP-HRD1 were applied to glutathione Sepharose 4B in a binding buffer containing 50 mM Tris-HCl (pH 7.5), 150 mM NaCl, 1 mM EDTA, 0.25% gelatin, and 1% Triton X-100 at 4°C for 16 h, and then washed with the buffer. T_NT reaction lysates producing ^{35}S-labeled Pael-R-FLAG were incubated with aliquots of GST- or GST-RP-HRD1-coupled glutathione-Sepharose 4B for 2 h at 4°C in the binding buffer. After extensive washing of the column with a washing buffer containing 10 mM Tris-HCl (pH 7.5), 150 mM NaCl, and 1% Triton X-100, the proteins recovered from the resin were subjected to SDS-PAGE followed by Coomassie blue staining and then visualized using an imaging analyzer (BAS-2500, Fujifilm).

RNA interference

For HRD1 knockdown by RNA interference, siGENOME SMARTpools of four oligoduplexes targeted against HRD1 (M-007090–00; Dharmacon Research, Lafayette, CO, USA) were used. Small interfering RNA (siRNA) transfection was performed using 100 pmol of siRNA and 7.5 μL of LipofectAMINE 2000 reagent (Invitrogen) in 6 cm dishes.

Results

Localization of HRD1 and Pael-R in the murine brain and cellular endoplasmic reticulum

As HRD1 has been shown to be highly expressed in the human fetal brain by RT-PCR-ELISA (Nagase *et al.* 2001), we immunohistochemically examined where HRD1 is localized in the murine brain. DAB staining showed HRD1 expression was observed in SNC neurons, which are selectively degenerated in Parkinson's disease (Fig. 1a), as well as in pyramidal cells of the hippocampus and Purkinje cells of the cerebellum (data not shown). Fluorescence staining using anti-NeuN and anti-GFAP antibodies showed that HRD1 was widely expressed in neuronal cells but not in glial cells (Fig. 1b). Furthermore, HRD1-immunoreactive cells were partially tyrosine hydroxylase-positive, indicating that HRD1 was expressed in dopaminergic neurons in the SNC (Fig. 1c). Thus, we hypothesized that HRD1 exists in the substantia nigra together with Pael-R as Pael-R is expressed in SNC dopaminergic neurons (Imai *et al.* 2001). To examine the subcellular localizations of HRD1 and Pael-R, expression vectors for HRD1-myc or the control vector (Mock) and Pael-R-FLAG were transfected into COS-1 cells. The localization of HRD1 (*green*) almost completely overlapped that of endogenous calreticulin (*red*) as revealed by an endoplasmic reticulum marker (Fig. 1d, lower). Pael-R (*red*) was widely localized in the endoplasmic reticulum as well as the cell surface and partially colocalized with HRD1 (*green*) in the endoplasmic reticulum (Fig. 1d, upper). Furthermore, endogenous HRD1 (*green*) was partially colocalized with Pael-R (*red*) in Pael-R-FLAG-expressing SH-SY5Y cells (Fig. 1e).

HRD1 interacts with unfolded Pael-R

When Pael-R was overexpressed in HEK293 cells, Pael-R proteins migrated as high molecular mass broad smears (Fig. 2a, lane 2), suggesting that they had undergone covalent modifications (glycosylation, ubiquitylation, etc.) (Imai *et al.* 2001); however, in the transfection of Pael-R with hemagglutinin-Ub, the ubiquitylation of Pael-R was barely observed in the absence of proteasome inhibitor MG132 (Fig. 2a, lane 5). Therefore, we presumed that the high molecular mass broad smears observed were the result of the aggregate formation of detergent-insoluble Pael-R rather than ubiquitylated Pael-R. Next, we used the immunoprecipitation method to investigate whether HRD1 interacts with Pael-R. HRD1 protein was detected in anti-FLAG antibody immunoprecipitates from cells cotransfected with HRD1-myc and Pael-R-FLAG (Fig. 2b, lane 15). In addition, Pael-R protein was detected in immunoprecipitates with an anti-myc antibody (Fig. 2b, lane 3), indicating that HRD1 interacts with Pael-R.

Furthermore, we performed coimmunoprecipitation in SH-SY5Y cells that stably expressed Pael-R-FLAG. The endogenous HRD1 protein was detected in immunoprecipitates with overexpressed aggregated Pael-R (Fig. 2c, upper and lower, lane 4). To investigate the interaction between HRD1 and Pael-R under a wider range of physiological conditions, the endogenous proteins in dopaminergic neuroblastoma SH-SY5Y cells were coimmunoprecipitated with the anti-Pael-R antibody; however, HRD1 was not coimmunoprecipitated with Pael-R (Fig. 2d, lane 3) under normal conditions. As Pael-R is easily unfolded and becomes insoluble under endoplasmic reticulum stress, we investigated the interaction

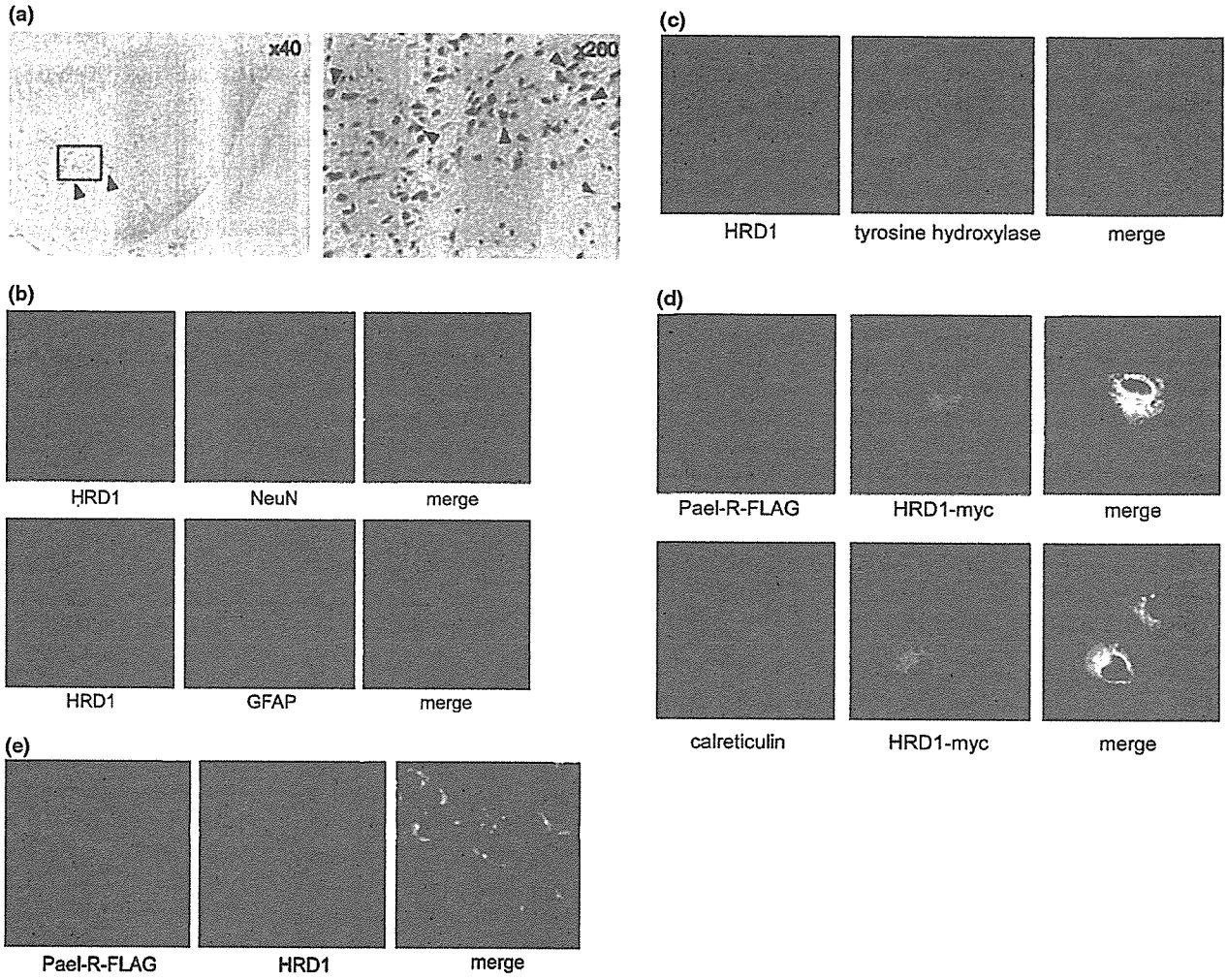

Fig. 1 Brain distribution and subcellular localization of Pael-R and HRD1. (a) Immunolocalization of HRD1 in the coronal section of the murine brain. HRD1 localization was detected by DAB immunostaining using anti-HRD1 polyclonal antibody (pAb). The magnification of the box in the left panel (×40) is part of the SNC, which is shown in the right panel (×200). The arrowheads indicate the expression of HRD1. (b) Localization of HRD1 in neurons and glia. The *green* signal (HRD1) was obtained with anti-HRD1 pAb and anti-rabbit IgG Alexa 488-conjugated secondary Ab, while the *red* signal (Pael-R) was obtained with either anti-NeuN monoclonal Ab (mAb; dentate gyrus; upper panel) or anti-GFAP mAb (CA4; lower panel) and anti-mouse IgG Alexa 546-conjugated secondary Ab. (c) Colocalization of HRD1 and tyrosine hydroxylase in the SNC of the coronal section of murine brain. HRD1 was detected by anti-HRD1 pAb (*green*); tyrosine hydroxylase was detected by antityrosine hydroxylase mAb (*red*). *Yellow* indicates the co-expression of H-RD1 in the SNC. (d) Colocalization of HRD1 and Pael-R in the endoplasmic reticulum. COS-1 cells were transiently transfected with HRD1-myc and Pael-R-FLAG. At 24 h after transfection, the cells were fixed and subjected to indirect immunofluorescence staining with anti-myc mAb and anti-FLAG pAb, or anti-calreticulin pAb. The *green* signal (HRD1) was obtained with anti-mouse IgG Alexa 488-conjugated secondary Ab and the *red* signal (Pael-R or calreticulin) with anti-rabbit IgG Alexa 594-conjugated secondary Ab. Superimposing the two colors (merge) resulted in a *yellow* signal, indicating the colocalization of the two proteins. (e) Colocalization of HRD1 and Pael-R in the endoplasmic reticulum of SH-SY5Y cells. The SH-SY5Y cells expressing Pael-R-FLAG were fixed and subjected to indirect immunofluorescence staining with anti-FLAG mAb (*red*) and anti-HRD1 pAb (*green*). The *green* signal (HRD1) was obtained with anti-rabbit IgG Alexa 488-conjugated secondary Ab and the *red* signal (Pael-R) with anti-mouse IgG Alexa 594-conjugated secondary Ab.

between Pael-R and HRD1 in native SH-SY5Y cells under endoplasmic reticulum stress. HRD1 was precipitated with Pael-R that tends to exist in an unfolded state under endoplasmic reticulum stress conditions (Fig. 2d, lane 4); this indicates that HRD1 interacts with the unfolded form of Pael-R.

HRD1 interacts with and ubiquitinates Pael-R through the proline-rich region

To investigate which HRD1 region interacts with Pael-R, a series of HRD1 mutants was prepared (Fig. 3a). HEK293 cells were transiently transfected with Pael-R-FLAG along with an empty vector (Mock), wild-type (wt)-HRD1-myc,

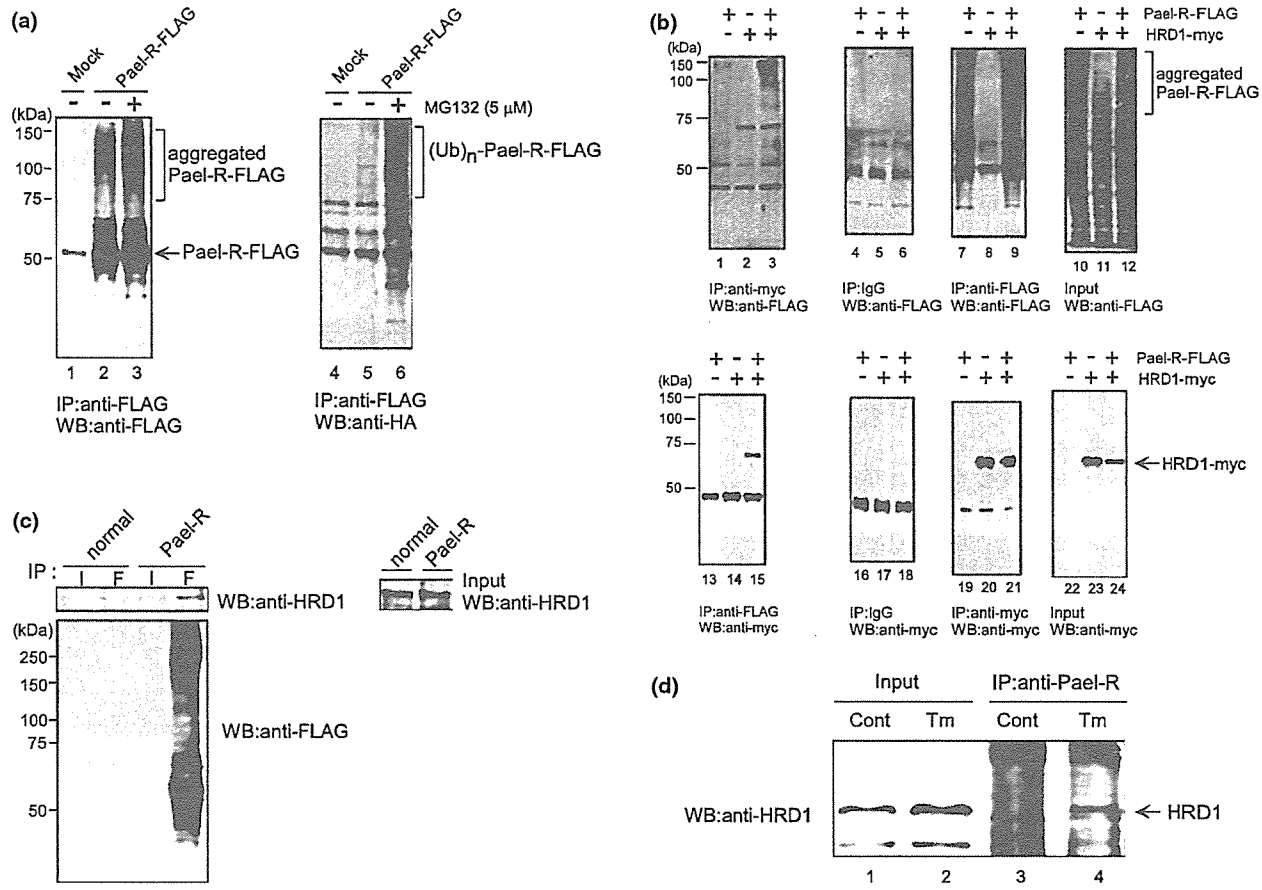

Fig. 2 Interaction of HRD1 with aggregated Pael-R. (a) Pael-R tends to exist in an aggregated form. HEK293 cells were transiently transfected with hemagglutinin-ubiquitin and an empty vector (Mock) or Pael-R-FLAG and incubated in the presence or absence of 5 μM MG132 (proteasome inhibitor). Equal amounts of proteins were immunoprecipitated with anti-FLAG mAb, and the immune complex was then analyzed by western blotting using anti-FLAG mAb (left) or anti-hemagglutinin pAb (right). (b) Interaction of Pael-R with HRD1 in HEK293 cells. HRD1 and Pael-R were coimmunoprecipitated in HEK293 cells transiently transfected with or without Pael-R-FLAG and HRD1-myc. At 48 h after transfection, the total cell lysates (Input) were analyzed by western blotting to check the expression of Pael-R and HRD1 proteins. Equal amounts of the proteins were immunoprecipitated with normal mouse IgG, anti-myc mAb, or anti-FLAG mAb. The immune complex was lysed in SDS sample buffer, resolved by SDS-PAGE, and analyzed by western blotting using anti-myc mAb or anti-FLAG mAb. (c) Endogenous HRD1 interacts with Pael-R in neuroblastoma SH-SY5Y cells stably expressing Pael-R-FLAG. The total cell lysates that stably expressed Pael-R-FLAG in neuroblastoma SH-SY5Y cells were analyzed by western blotting using anti-HRD1 pAb (Input, right panel). Equal amounts of the proteins were immunoprecipitated with normal mouse IgG (I) or anti-FLAG mAb (F), and the immune complex was then analyzed by western blotting using anti-HRD1 pAb (left panel, upper) or anti-FLAG mAb (right panel, lower). (d) Endogenous interaction of HRD1 with Pael-R in tunicamycin-treated neuroblastoma SH-SY5Y cells. The SH-SY5Y cells were either untreated (control) or treated (tunicamycin) with 2.5 μg/mL tunicamycin for 24 h. The total cell lysates (Input, lanes 1 and 2) were analyzed by western blotting to check the expression of HRD1 proteins. Equal amounts of proteins were immunoprecipitated with anti-Pael-R pAb. The immune complex was analyzed by western blotting by using anti-HRD1 pAb (IP, lanes 3 and 4; Abgent).

membrane (M)-HRD1 Δmembrane (ΔM)-HRD1-myc, or membrane-RING (MR)-HRD1-myc. Wt-HRD1 and ΔM-HRD1 were detected in immunoprecipitates with anti-FLAG, whereas (M)-HRD1 and (MR)-HRD1 were not detected (Fig. 3b, upper, lanes 3, 5), suggesting that HRD1 requires a proline-rich region for association with Pael-R. We examined whether Pael-R interacts with the proline-rich region of HRD1 *in vitro* (Fig. 4a). In an *in vitro* GST pull-down assay, RP-HRD1 bound to both the native and aggregated forms of Pael-R (Fig. 4a, upper, lane 5). Thus, HRD1 may directly interact with Pael-R through the proline-rich region.

We then evaluated whether HRD1 ubiquitinates Pael-R through its E3 activity *in vitro*. Using RP-HRD1-myc and Pael-R-FLAG generated by *in vitro* translations (Fig. 4b), we examined whether Pael-R is ubiquitylated by RP-HRD1 *in vitro*. Recombinant E2 UbcH5c was used in this assay as HRD1 is shown to be ubiquitylated by UbcH5c *in vitro* (Nadav *et al.* 2003; Kikkert *et al.* 2004). *In vitro* transcrip-

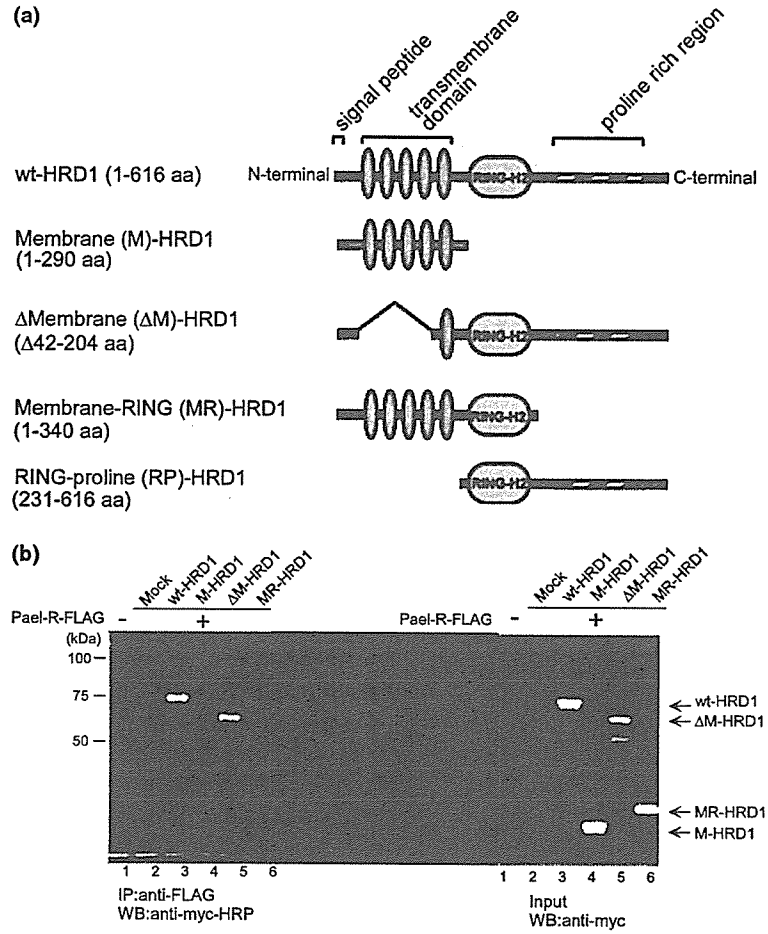

Fig. 3 Interaction of Pael-R with HRD1 and its mutants. (a) Schematic representation of the HRD1 constructs. The panel diagrammatically represents wild-type HRD1 and a variety of HRD1 mutants used to determine the Pael-R binding domain. Numbers in parentheses indicate the corresponding amino acid residues of HRD1. (b) Coimmunoprecipitation of Pael-R and a variety of HRD1 mutants. Coimmunoprecipitation was performed in HEK293 cells transiently transfected with Pael-R-FLAG and an empty vector (Mock), wild-type (wt)-HRD1-myc, membrane (M)-HRD1-myc, Δmembrane (ΔM)-HRD1-myc or membrane-RING (MR)-HRD1-myc. At 48 h after transfection, the total cell lysates (Input) were analyzed by western blotting using antimyc mAb (right). Equal amounts of the proteins were immunoprecipitated with anti-FLAG mAb, and the immune complex was then analyzed by western blotting using antimyc mAb (left).

tion/translation reaction lysates containing RP-HRD1 and Pael-R were incubated with other components including E1 (rabbit), E2 (GST-UbcH5c), and GST-ubiquitin. Pael-R-FLAG proteins were ubiquitylated only in the presence of RP-HRD1 along with all other components (Fig. 4c, lane 6), indicating that HRD1 directly interacts with and ubiquitinates Pael-R.

HRD1 degrades unfolded Pael-R

We investigated whether HRD1 accelerates Pael-R degradation via the UPS. Normal HEK293 cells and those stably expressing wt-HRD1 or M-HRD1 were transiently transfected with Pael-R-FLAG. Equal amounts of proteins were immunoprecipitated with anti-FLAG monoclonal antibody and subjected to western blotting. Pael-R and its high molecular mass broad smears were markedly decreased in wt-HRD1-expressing cells (Fig. 5a, first panel, lanes 5, 6). MG132 inhibited the decrease of Pael-R protein (Fig. 5a, first panel, lane 7), indicating that HRD1 promoted the degradation of Pael-R via the UPS. In contrast, Pael-R was not degraded by M-HRD1, which has no RING-finger domain and lacks E3 activity (Fig. 5a, first panel, lanes 8, 9). To confirm that these results were not caused by a decrease in the transfection or transcription efficiency of Pael-R, the expression level of Pael-R mRNA was examined by RT-PCR using the total RNA of the cells used in western blotting. In each clone, the expression levels of transfected Pael-R were almost equal (Fig. 5a, third panel); furthermore, another clone stably expressing wt-HRD1 degraded Pael-R (data not shown).

To immunocytochemically visualize the degradation of Pael-R by HRD1, normal HEK293 cells and those stably

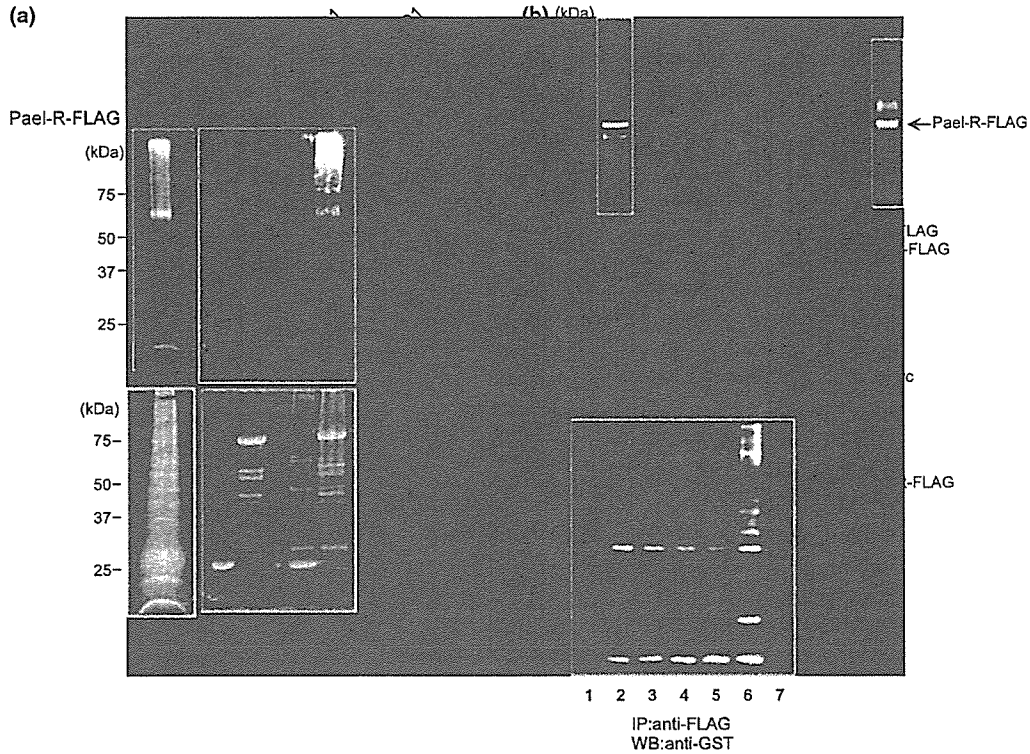

Fig. 4 HRD1 ubiquitinates Pael-R *in vitro*. (a) Coimmunoprecipitation of Pael-R with RING-proline (RP)-HRD1 *in vitro*. GST-fused RP-HRD1 or GST alone was bound to glutathione beads incubated with [^{35}S]-labeled Pael-R generated by an *in vitro* transcription/translation system. After extensive washing, the protein-bound beads were resolved by SDS-PAGE followed by Coomassie blue staining (lower), and detected by autoradiography (upper). (b) Protein products of Pael-R and RP-HRD1. Western blotting analysis of the components used for *in vitro* ubiquitylation assays. RP-HRD1-myc and Pael-R-FLAG were produced by a T_NT quick-coupled transcription/translation system. T_NT reaction lysates containing RP-HRD1 were analyzed by western blotting using anti-myc mAb (left), whereas T_NT reaction lysates containing Pael-R were immunoprecipitated with anti-FLAG mAb. The immune complex was then analyzed by western blotting using anti-FLAG mAb (right). (c) *In vitro* ubiquitylation assay. Western blotting analysis of the *in vitro* ubiquitylation reactions mediated by HRD1 with anti-GST pAb. T_NT reaction lysates containing RP-HRD1 and Pael-R were mixed with other components including E1 (rabbit), E2 (GST-UbcH5c), or GST-ubiquitin in the reaction buffer. The reaction lysates were then incubated at 30°C for 90 min, immunoprecipitated with anti-FLAG mAb, and analyzed by western blotting using anti-GST pAb.

expressing wt-HRD1 or M-HRD1 were transfected with Pael-R-FLAG and DsRED, a red fluorescent protein. The amount of Pael-R-FLAG protein decreased in cells expressing wt-HRD1-myc compared with control cells, whereas the amount of Pael-R-FLAG protein in cells expressing M-HRD1-myc and in control cells was similar (Fig. 5b, upper, *green*). The red signals (lower panels) were DsRED proteins cotransfected with Pael-R-FLAG for use as transfection controls. These results indicate that HRD1 degrades Pael-R by its E3 activity.

Next, the degradation of Pael-R by HRD1 was examined by performing a pulse-chase experiment. The levels of ^{35}S-labeled Pael-R were plotted relative to the amount present at time 0 (Fig. 5c). Following a 3 h chase, 54.4% and 52.0% of *de novo* synthesized Pael-R remained in cells transfected with Mock and M-HRD1, respectively. In contrast, Pael-R degradation in HRD1-transfected cells was accelerated such that at 3 h, 28.7% of proteins remained, indicating that HRD1 accelerates the degradation of newly synthesized Pael-R protein.

Furthermore, to investigate whether HRD1 is involved in the physiological degradation of Pael-R, we examined the effect of HRD1 suppression by siRNA on Pael-R accumulation in SH-SY5Y cells stably expressing Pael-R-FLAG. The amount of the aggregated form of Pael-R was increased by the suppression of HRD1 expression (Fig. 5d, upper, lane 2) whereas the native form was not affected markedly; thus, it is possible that endogenous HRD1 preferentially degrades aggregated Pael-R but not native Pael-R.

α-Synuclein is a component of Lewy bodies in Parkinson's disease (Trojanowski *et al.* 1998), and a 22-kD glycosylated form of α-synuclein is reported to be ubiquitylated by Parkin (Shimura *et al.* 2001), and is ubiquitylated when overexpressed in cells (Imai *et al.* 2000). Unfolded α-synuclein can be degraded by the 20S proteasome *in vitro* (Tofaris *et al.* 2001). We examined whether α-synuclein, like Pael-R, is a

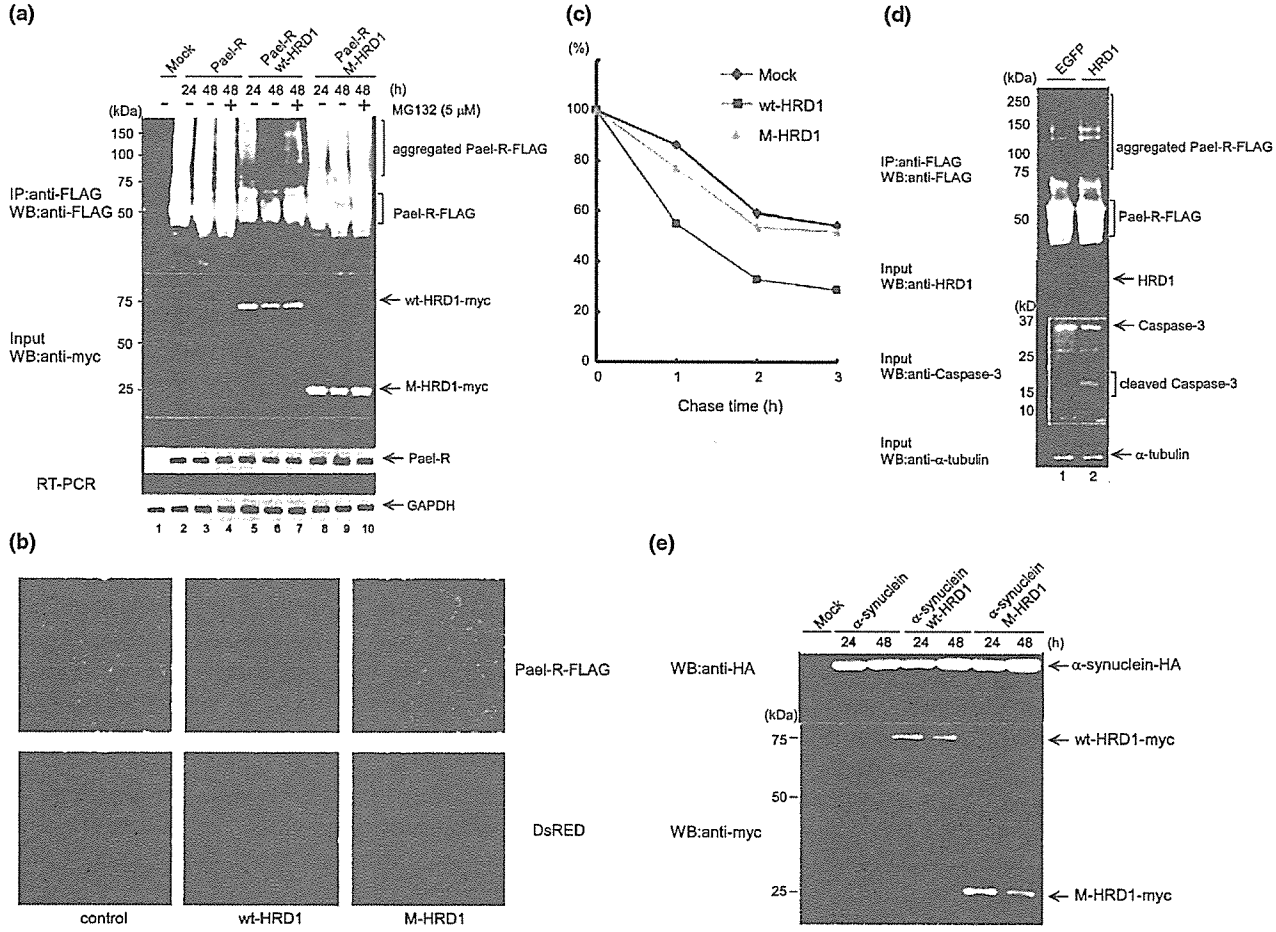

Fig. 5 Degradation of Pael-R by HRD1. (a) HEK293 cells stably expressing wt-HRD1 or M-HRD1 were transiently transfected with Pael-R-FLAG and incubated for the indicated periods in the presence or absence of 5 μM MG132, which was added 12 h before cell harvest. The total cell lysates (Input) were analyzed by western blotting using anti-myc mAb (middle). Equal amounts of the proteins were immunoprecipitated with anti-FLAG mAb, and the immune complex was then analyzed by western blotting using anti-FLAG mAb (upper). The total RNA of the cells used in western blotting was prepared and subjected to RT-PCR (lower). (b) HEK293 cells stably expressing wt-HRD1 or M-HRD1 were transiently transfected with Pael-R-FLAG and DsRED (red fluorescent protein). At 36 h after transfection, the cells were fixed and subjected to indirect immunofluorescence staining with anti-FLAG mAb (upper). The *green* signal (Pael-R) was obtained with anti-mouse IgG Alexa 488-conjugated secondary Ab while the *red* signal (lower) shows DsRED proteins used as a transfection control. (c) Pulse-chase assay. Neuro2a cells were transiently transfected with Pael-R-FLAG and an empty vector (Mock), wt-HRD1, or M-HRD1. At 36 h after transfection, cells were pulse-labeled with [^{35}S]-methionine/cysteine and chased for the indicated periods. Equal amounts of [^{35}S]-labeled Pael-R and M-HRD1 were immunoprecipitated with anti-FLAG mAb; the immune complex was then lysed in SDS sample buffer, resolved by SDS-PAGE, detected by autoradiography, and quantified by phosphorimaging. The levels of [^{35}S]-labeled Pael-R are plotted relative to the amount present at time 0. (d) Induction of aggregated Pael-R accumulation and caspase activation by inhibition of HRD1 expression. SH-SY5Y cells stably expressing Pael-R-FLAG were transiently transfected with the siRNA of enhanced green fluorescent protein (EGFP, control) or HRD1, and incubated for 72 h. The total cell lysates were analyzed by western blotting using anti-HRD1 pAb (2nd panel), anti-caspase-3 pAb (3rd panel), and anti-α-tubulin mAb (5th panel). Equal amounts of the proteins were immunoprecipitated with anti-FLAG mAb, and the immune complex was then analyzed by western blotting using anti-FLAG mAb (1st panel). (e) HRD1 did not degrade α-synuclein. HEK293 cells stably expressing wt-HRD1 or M-HRD1 were transiently transfected with α-synuclein-hemagglutinin and incubated for the indicated periods. The total cell lysates were analyzed by western blotting using anti-hemagglutinin pAb (upper) or anti-myc mAb (lower).

substrate of HRD1. Normal HEK293 cells and those stably expressing wt- or M-HRD1 were transiently transfected with α-synuclein-hemagglutinin. The protein levels of α-synuclein were not changed by HRD1 (Fig. 5e, upper), indicating that α-synuclein is not a substrate of HRD1.

HRD1 suppresses Pael-R-induced cell death

The accumulation of Pael-R causes endoplasmic reticulum stress and subsequent cell death. We investigated whether HRD1 suppresses Pael-R-induced cell death. Normal HEK293 cells and those stably expressing wt- or M-HRD1

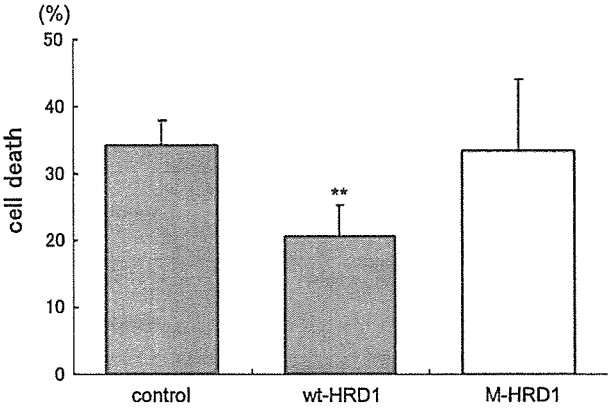

Fig. 6 HRD1 protects against Pael-R-induced cell death. HEK293 cells (control) and HEK 293 cells stably expressing wt-HRD1 or M-HRD1 were transiently transfected with a control vector (Mock) or Pael-R-FLAG and incubated for 24 h. The cells were washed with PBS and then stained with crystal violet (0.1%) for 20 min, and the wells were washed with water and air-dried. The dye was eluted with water containing 0.5% SDS for 20 min, and the optical density at 590 nm was measured. The percentage of cell death was calculated as follows: 100 – [(OD for assay/OD for control well) × 100]. The results obtained from each cell transfected with Pael-R-FLAG were compared with those obtained from cells transfected with Mock. The results are expressed as the means ± SD (three independent experiments in duplicate). Statistical analysis was performed with Student's *t*-test (**$p < 0.01$, vs. normal).

were transiently transfected with a control vector (Mock) or Pael-R-FLAG and incubated for 24 h. The cell death of HEK293 was compared with that of cells transfected with the control vector. The crystal violet assay showed that wt-HRD1-expressing cells were more resistant to Pael-R overexpression than control and M-HRD1 cells (control, 34.3%; wt-HRD1, 20.8%; M-HRD1, 33.4%) (Fig. 6). Furthermore, we found that the accumulation of aggregated Pael-R induced by the repression of HRD1 in SH-SY5Y cells that stably expressed Pael-R-FLAG promoted a decrease in pro-caspase-3 and an increase in cleaved caspase-3 (Fig. 5d, third panel, lane 2), which indicates the activation of caspase-3 and subsequent apoptosis. These results indicate that HRD1 suppresses apoptosis induced by Pael-R accumulation.

Involvement of HRD1 in the degradation of Pael-R induced by ATF6

We found that ATF6 induced the expression of HRD1 (Kaneko *et al.* 2002; unpublished data). As ATF6-mediated UPR possibly induces a number of ERAD genes, we speculated that the degradation of Pael-R is promoted by ATF6. HEK293 cells were transiently transfected with Pael-R-FLAG and either an empty vector (Mock) or hemagglutinin-ATF6 (1–373; cytoplasmic domain worked as a transcription factor), and incubated for 48 h in the presence or absence of MG132. The amount of both native and aggregated Pael-R decreased in cells expressing ATF6

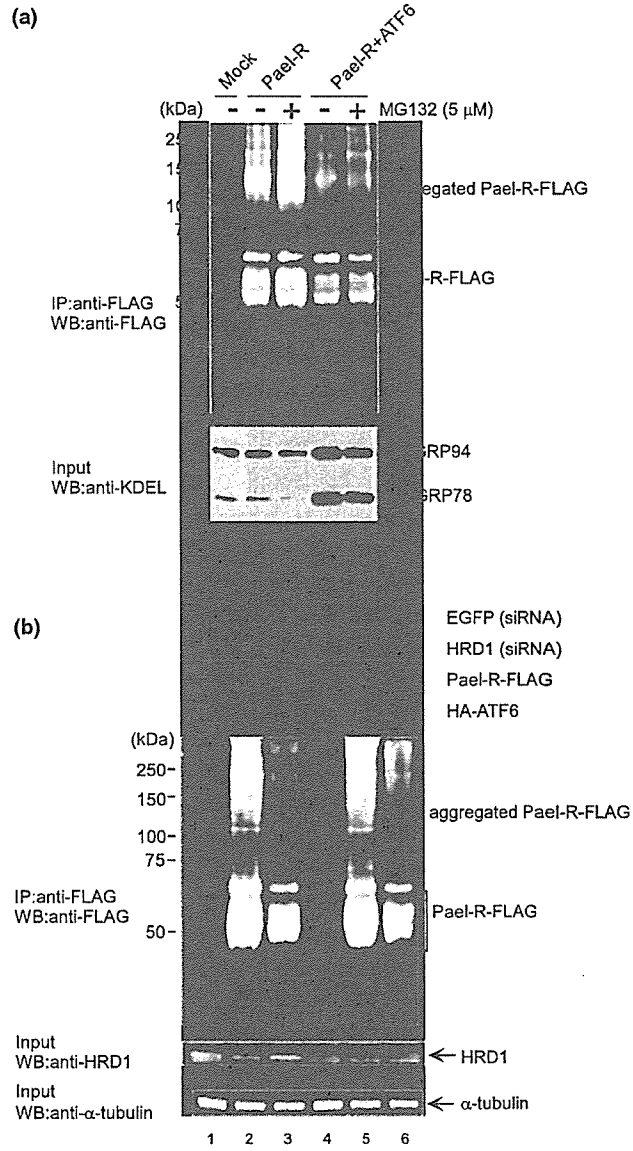

Fig. 7 Degradation of Pael-R promoted by ATF6. (a) HEK293 cells were transiently transfected with an empty vector (Mock) or Pael-R-FLAG with or without hemagglutinin-ATF6 (cleaved form); they were incubated for 48 h in the presence or absence of 5 μM MG132 (12 h incubation). The total cell lysates (Input) were analyzed by western blotting using anti-KDEL mAb (lower). Equal amounts of the proteins were immunoprecipitated with anti-FLAG mAb, and then analyzed by western blotting using anti-FLAG mAb (upper). (b) Involvement of HRD1 in ATF6-mediated Pael-R degradation. HEK293 cells were transiently transfected with Pael-R-FLAG and hemagglutinin-ATF6 (cleaved form) and siRNA of EGFP (control) or HRD1 and incubated for 30 h. The total cell lysates (Input) were analyzed by western blotting using anti-HRD1 pAb (middle) or anti-α-tubulin mAb (lower). Equal amounts of the proteins were immunoprecipitated with anti-FLAG mAb, and the immune complex was then analyzed by western blotting using anti-FLAG mAb (upper).

(Fig. 7a, upper, lane 4); moreover, MG132 inhibited the decrease in Pael-R protein by ATF6 overexpression (Fig. 7a, upper, lane 5). The increased expression of glucose-regulated proteins GRP78 and GRP94 indicates the induction of UPR by ATF6 (Fig. 7a, lower, lanes 4, 5). These results indicate that the up-regulation of UPR by ATF6 leads to the degradation of Pael-R proteins via the UPS; however, it is not known which proteins induced by ATF6 are involved in this degradation.

To determine whether HRD1 is involved in the degradation of Pael-R induced by UPR up-regulation, we investigated the effect of HRD1 suppression by siRNA on degradation. HEK293 cells were transiently transfected with Pael-R-FLAG, hemagglutinin-ATF6, and either green fluorescent protein (GFP) (siRNA) or HRD1 (siRNA). ATF6 induced HRD1 expression (Fig. 7B, lower, lane 3), whereas HRD1 repression partially suppressed the ATF6-induced decrease in the number of Pael-R aggregates, but not the amount of the native form (Fig. 7b, upper, lane 6), suggesting that UPR-induced HRD1 preferentially promotes the degradation of unfolded Pael-R.

Discussion

In this report, we found that HRD1 was expressed in the dopaminergic neurons of the SNC, colocalized with Pael-R in the endoplasmic reticulum, and directly interacted with Pael-R at the proline-rich region of HRD1. We showed that HRD1 promoted the ubiquitylation and degradation of Pael-R; additionally, the activation of UPR by ATF6 induced Pael-R degradation, which partially depends on HRD1.

First, we found that HRD1 was locally expressed in SNC neurons, including dopaminergic neurons, of the murine brain. Pael-R is reportedly expressed in SNC neurons, implying that HRD1 and Pael-R are colocalized in dopaminergic neurons in the SNC. Parkin, an E3, is up-regulated in response to endoplasmic reticulum stress and protects cells via ERAD from endoplasmic reticulum stress-induced apoptosis (Imai *et al.* 2000). Pael-R accumulates in the brains of AR-JP patients and induces endoplasmic reticulum stress, possibly because of Parkin mutation (Imai *et al.* 2001). Furthermore, it has been reported that Pael-R overexpression causes the selective degeneration of dopaminergic neurons in *Drosophila* and that the coexpression of human Parkin suppresses Pael-R toxicity by degrading Pael-R. It has also been reported that interference in endogenous *Drosophila* Parkin functions enhances Pael-R toxicity (Yang *et al.* 2003). On the other hand, we previously reported that human HRD1 is up-regulated in response to endoplasmic reticulum stress. It possesses E3 activity and protects against endoplasmic reticulum stress-induced cell death (Kaneko *et al.* 2002), suggesting that HRD1 can degrade protein substrates accumulated during endoplasmic reticulum stress. There is, however, little information regarding these substrates, with the exception of CD-3α and TCR-α, and HMG-CoA reductase (Kikkert *et al.* 2004). We showed that HRD1 was colocalized in the endoplasmic reticulum with Pael-R and they interacted at endogenous levels as well as overexpression levels. We therefore hypothesized that HRD1, like Parkin, may degrade Pael-R and suppress cell death caused by Pael-R accumulation.

We found that endogenous HRD1 interacted with not only overexpressed Pael-R but also endogenous Pael-R under endoplasmic reticulum stress conditions. Pael-R tends to exist in an unfolded state when it is overexpressed or when subjected to endoplasmic reticulum stress; therefore, it is likely that HRD1 preferentially interacts with the unfolded form of Pael-R but not with the normally folded form. Therefore, it can be speculated that unfolded Pael-R is recognized by acceptors of terminally misfolded glycoproteins, such as endoplasmic reticulum degradation-enhancing alpha-mannosidase-like protein (EDEM), and is destined to be eliminated from the endoplasmic reticulum (Molinari *et al.* 2003; Oda *et al.* 2003); HRD1 then binds to Pael-R passing through the translocon in the endoplasmic reticulum membrane by its proline-rich region and ubiquitinates the unfolded form of Pael-R. If this is true, it is unlikely that HRD1 directly associates with and ubiquitinates native Pael-R on the endoplasmic reticulum membrane without mediation of the translocon.

On the other hand, we showed that the high molecular mass broad smears of Pael-R mostly comprised not ubiquitylated forms, but possibly glycosylated or aggregated forms, as previously reported (Imai *et al.* 2001). The inhibition of HRD1 expression by siRNA induced the accumulation of smears and the activation of caspase-3. Therefore, it is likely that HRD1 preferentially ubiquitinates and degrades unfolded Pael-R to prevent the accumulation of aggregated Pael-R that leads to endoplasmic reticulum stress-induced apoptosis.

We further showed that HRD1 interacted with Pael-R at its proline-rich region and ubiquitylated Pael-R *in vitro*, indicating direct interaction between the proline-rich region of HRD1 and Pael-R. Yeast Hrd1p has no proline-rich region, whereas human HRD1 contains a proline-rich region similar to that seen in the Cbl family of ubiquitin ligases (Fujita *et al.* 2002). It has been reported that the proline-rich region is essential for protein–protein interaction and that the RING-finger and proline-rich regions are sufficient for the binding and ubiquitylation of substrates (Fang *et al.* 2001). Therefore, human HRD1 appears to interact with substrates at the proline-rich region and ubiquitinates the substrates at the RING-finger domain. On the other hand, Hrd1p degrades Hmg2p, one of the yeast isozymes of HMG-CoA reductase, despite the lack of a proline-rich region (Gardner *et al.* 2000). Thus, we propose that in the course of evolution, human HRD1 acquired a proline-rich region to interact with and ubiquitinate a variety of substrates; whether other

substrates are bound to the proline-rich region remains to be determined.

We investigated whether α-synuclein is a substrate of HRD1. An α-synuclein mutant (Ala53Thr or Ala30Pro) has been reported in the brain of Parkinson's disease patients, promoting protofibril formation relative to wild-type α-synuclein (Conway *et al.* 2000). Parkin ubiquitinates the *O*-glycosylated form (αSp22) (Shimura *et al.* 2001) and suppresses the toxicity of normal or pathogenic alpha-synuclein (Petrucelli *et al.* 2002; Yang *et al.* 2003; Lo Bianco *et al.* 2004; Haywood and Staveley 2004). HRD1 did not degrade wild-type α-synuclein, probably due to the different localization or binding ability of HRD1 and α-synuclein; however, whether HRD1 degrades α-synuclein mutants or the *O*-glycosylated form remains to be clarified. On the other hand, Hrd3p, another UPR-inducible ERAD protein, has been reported to interact with Hrd1p and mediate the regulation of Hrd1p stability and activity in yeast (Gardner *et al.* 2000). We have identified SEL1 as a candidate human homolog of Hrd3p and have found that SEL1 interacted with human HRD1 (data not shown). We have further found that HRD1 did not degrade SEL1 despite this interaction; rather, the amount of SEL1 increased in the presence of HRD1 (data not shown). Based on these observations, we speculate that HRD1 specifically increases the degradation of proteins.

When unfolded proteins accumulate in the endoplasmic reticulum, the UPR is activated by ATF6 and IRE1, resulting in the induction of several endoplasmic reticulum chaperones and ERAD components (Travers *et al.* 2000; Lee *et al.* 2003). Therefore, we hypothesized that ATF6 promotes the degradation of Pael-R by inducing UPR genes including HRD1, although ATF6 can induce a variety of genes in addition to HRD1. Interestingly, ATF6 induced the degradation of both aggregated and unaggregated Pael-R, whereas the suppression of ATF6-induced HRD1 expression by siRNA caused an increase in the aggregated form. Thus, it is likely that endogenous HRD1 preferentially recognizes and degrades the unfolded forms of Pael-R. Based on these results, we propose that after the accumulation of unfolded Pael-R due to stress or Parkin mutation, ATF6 and/or IRE1-XBP1 pathways are activated and induce UPR genes including HRD1; this promotes the folding or degradation of unfolded Pael-R to prevent unfolded Pael-R-induced cell death (Fig. 8).

It has been reported that Parkin knockout mice exhibit little change in movement ability or the neurons of the substantia nigra (Itier *et al.* 2003; Goldberg *et al.* 2003; von Coelln *et al.* 2004; Perez and Palmiter 2005). We therefore speculate that HRD1 degrades Pael-R and possibly other proteins to balance the unfolded protein accumulation caused by Parkin gene mutation; nonetheless, it is possible that other unknown E3s participate in this degradation in the absence of Parkin, although the reason behind the loss of dopaminergic neurons in AR-JP patients but not in Parkin knockout mice remains unknown despite the similarity in the functional loss of Parkin. On the other hand, it is likely that HRD1 ubiquitinates not only Pael-R but also other substrates related to conformational diseases caused by the accumulation of unfolded proteins as HRD1 can suppress global endoplasmic reticulum stress induced by various chemical reagents.

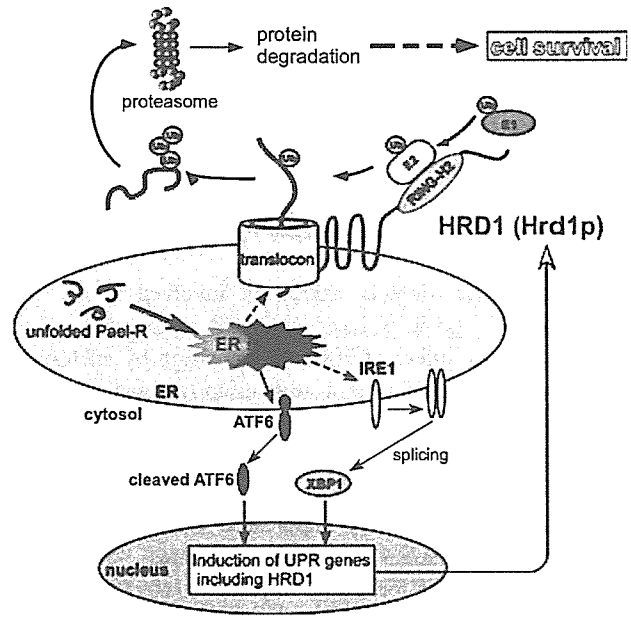

Fig. 8 A hypothetical model demonstrating how HRD1 participates in the degradation of unfolded Pael-R. When unfolded Pael-R is accumulated in the endoplasmic reticulum, ATF6 and IRE1-XBP1 pathways are activated, and UPR genes including HRD1 are then induced. HRD1 degrades unfolded Pael-R and suppresses Pael-R-induced cell death.

Acknowledgements

We are grateful to Dr. Yuzuru Imai for his helpful discussions. We thank Otsuka GEN Research Institute for providing the HRD1 antibody. We also thank Dr. Takahiro Taira and Mr. Takanori Tabata for their helpful discussions. We thank Mr. T. Itou, Mitsubishi Chemical Safety Institute, LTD. for pertinent advises on immunohistochemical study. This study was supported by Grants-in-Aid for Scientific Research from the Ministry of Education, Culture, Sports, Science and Technology, Japan.

References

Amano T., Yamasaki S., Yagishita N. *et al.* (2003) Synoviolin/Hrd1, an E3 ubiquitin ligase, as a novel pathogenic factor for arthropathy. *Genes Dev.* **17**, 2436–2449.

Conway K. A., Lee S. J., Rochet J. C., Ding T. T., Williamson R. E. and Lansbury P. T. Jr (2000) Acceleration of oligomerization, not fibrillization, is a shared property of both alpha-synuclein muta-

tions linked to early-onset Parkinson's disease: implications for pathogenesis and therapy. *Proc. Natl Acad. Sci. U S A* **97**, 571–576.

Cox J. S., Shamu C. E. and Walter P. (1993) Transcriptional induction of genes encoding endoplasmic reticulum resident proteins requires a transmembrane protein kinase. *Cell* **73**, 1197–1206.

Deak P. M. and Wolf D. H. (2001) Membrane topology and function of Der3/Hrd1p as a ubiquitin-protein ligase (E3) involved in endoplasmic reticulum degradation. *J. Biol. Chem.* **276**, 10 663–10 669.

Fang D., Wang H. Y., Fang N., Altman Y., Elly C. and Liu Y. C. (2001) Cbl-b, a RING-type E3 ubiquitin ligase, targets phosphatidylinositol 3-kinase for ubiquitination in T cells. *J. Biol. Chem.* **276**, 4872–4878.

Friedlander R., Jarosch E., Urban J., Volkwein C. and Sommer T. (2000) A regulatory link between ER-associated protein degradation and the unfolded protein response. *Nat. Cell Biol.* **2**, 379–384.

Fujita Y., Krause G., Scheffner M., Zechner D., Leddy H. E., Behrens J., Sommer T. and Birchmeier W. (2002) Hakai, a c-Cbl-like protein, ubiquitinates and induces endocytosis of the E-cadherin complex. *Nat. Cell Biol.* **4**, 222–231.

Gardner R. G., Swarbrick G. M., Bays N. W., Cronin S. R., Wilhovsky S., Seelig L., Kim C. and Hampton R. Y. (2000) Endoplasmic reticulum degradation requires lumen to cytosol signaling. Transmembrane control of Hrd1p by Hrd3p. *J. Cell Biol.* **151**, 69–82.

Gardner R. G., Shearer A. G. and Hampton R. Y. (2001) In vivo action of the HRD ubiquitin ligase complex: mechanisms of endoplasmic reticulum quality control and sterol regulation. *Mol. Cell Biol.* **21**, 4276–4291.

Goldberg M. S., Fleming S. M., Palacino J. J. *et al.* (2003) Parkin-deficient mice exhibit nigrostriatal deficits but not loss of dopaminergic neurons. *J. Biol. Chem.* **278**, 43 628–43 635.

Haywood A. F. and Staveley B. E. (2004) Parkin counteracts symptoms in a Drosophila model of Parkinson's disease. *BMC Neurosci.* **5**, 14.

Haze K., Yoshida H., Yanagi H., Yura T. and Mori K. (1999) Mammalian transcription factor ATF6 is synthesized as a transmembrane protein and activated by proteolysis in response to endoplasmic reticulum stress. *Mol. Biol. Cell* **10**, 3787–3799.

Hershko A. and Ciechanover A. (1998) The ubiquitin system. *Annu. Rev. Biochem.* **67**, 425–479.

Imai Y., Soda M. and Takahashi R. (2000) Parkin suppresses unfolded protein stress-induced cell death through its E3 ubiquitin-protein ligase activity. *J. Biol. Chem.* **275**, 35 661–35 664.

Imai Y., Soda M., Inoue H., Hattori N., Mizuno Y. and Takahashi R. (2001) An unfolded putative transmembrane polypeptide, which can lead to endoplasmic reticulum stress, is a substrate of Parkin. *Cell* **105**, 891–902.

Itier J. M., Ibanez P., Mena M. A. *et al.* (2003) Parkin gene inactivation alters behaviour and dopamine neurotransmission in the mouse. *Hum. Mol. Genet.* **12**, 2277–2291.

Kaneko M., Ishiguro M., Niinuma Y., Uesugi M. and Nomura Y. (2002) Human HRD1 protects against ER stress-induced apoptosis through ER-associated degradation. *FEBS Lett.* **532**, 147–152.

Kaufman R. J. (1999) Stress signaling from the lumen of the endoplasmic reticulum: coordination of gene transcriptional and translational controls. *Genes Dev.* **13**, 1211–1233.

Kaufman R. J., Scheuner D., Schroder M., Shen X., Lee K., Liu C. Y. and Arnold S. M. (2002) The unfolded protein response in nutrient sensing and differentiation. *Nat. Rev. Mol. Cell Biol.* **3**, 411–421.

Kikkert M., Doolman R., Dai M., Avner R., Hassink G., van Voorden S., Thanedar S., Roitelman J., Chau V. and Wiertz E. (2004) Human HRD1 is an E3 ubiquitin ligase involved in degradation of proteins from the endoplasmic reticulum. *J. Biol. Chem.* **279**, 3525–3534.

Kitada T., Asakawa S., Hattori N., Matsumine H., Yamamura Y., Minoshima S., Yokochi M., Mizuno Y. and Shimizu N. (1998) Mutations in the parkin gene cause autosomal recessive juvenile parkinsonism. *Nature* **392**, 605–608.

Lee A. H., Iwakoshi N. N. and Glimcher L. H. (2003) XBP-1 regulates a subset of endoplasmic reticulum resident chaperone genes in the unfolded protein response. *Mol. Cell. Biol.* **23**, 7448–7459.

Lo Bianco C., Schneider B. L., Bauer M., Sajadi A., Brice A., Iwatsubo T. and Aebischer P. (2004) Lentiviral vector delivery of parkin prevents dopaminergic degeneration in an alpha-synuclein rat model of Parkinson's disease. *Proc. Natl Acad. Sci. U S A* **101**, 17 510–17 515.

Mizuno Y., Hattori N. and Matsumine H. (1998) Neurochemical and neurogenetic correlates of Parkinson's disease. *J. Neurochem.* **71**, 893–902.

Molinari M., Calanca V., Galli C., Lucca P. and Paganetti P. (2003) Role of EDEM in the release of misfolded glycoproteins from the calnexin cycle. *Science* **299**, 1397–1400.

Murakami T., Shoji M., Imai Y., Inoue H., Kawarabayashi T., Matsubara E., Harigaya Y., Sasaki A., Takahashi R. and Abe K. (2004) Pael-R. is accumulated in Lewy bodies of Parkinson's disease. *Ann. Neurol.* **55**, 439–442.

Nadav E., Shmueli A., Barr H., Gonen H., Ciechanover A. and Reiss Y. (2003) A novel mammalian endoplasmic reticulum ubiquitin ligase homologous to the yeast Hrd1. *Biochem. Biophys. Res. Commun.* **303**, 91–97.

Nagase T., Nakayama M., Nakajima D., Kikuno R. and Ohara O. (2001) Prediction of the coding sequences of unidentified human genes. XX. The complete sequences of 100 new cDNA clones from brain which code for large proteins in vitro. *DNA Res.* **8**, 85–95.

Oda Y., Hosokawa N., Wada I. and Nagata K. (2003) EDEM as an acceptor of terminally misfolded glycoproteins released from calnexin. *Science* **299**, 1394–1397.

Palacino J. J., Sagi D., Goldberg M. S., Krauss S., Motz C., Wacker M., Klose J. and Shen J. (2004) Mitochondrial dysfunction and oxidative damage in parkin-deficient mice. *J. Biol. Chem.* **279**, 18 614–18 622.

Perez F. A. and Palmiter R. D. (2005) Parkin-deficient mice are not a robust model of parkinsonism. *Proc. Natl Acad. Sci. U S A.* **102**, 2174–2179.

Periquet M., Corti O., Jacquier S. and Brice A. (2005) Proteomic analysis of parkin knockout mice: alterations in energy metabolism, protein handling and synaptic function. *J. Neurochem.* **95**, 1259–1276.

Petrucelli L., O'Farrell C., Lockhart P. J., Baptista M., Kehoe K., Vink L., Choi P., Wolozin B., Farrer M., Hardy J. and Cookson M. R. (2002) Parkin protects against the toxicity associated with mutant alpha-synuclein: proteasome dysfunction selectively affects catecholaminergic neurons. *Neuron.* **36**, 1007–1019.

Plemper R. K., Bordallo J., Deak P. M., Taxis C., Hitt R. and Wolf D. H. (1999) Genetic interactions of Hrd3p and Der3p/Hrd1p with Sec61p suggest a retro-translocation complex mediating protein transport for ER degradation. *J. Cell Sci.* **112**, 4123–4134.

Shen J., Chen X., Hendershot L. and Prywes R. (2002) ER stress regulation of ATF6 localization by dissociation of BiP/GRP78 binding and unmasking of Golgi localization signals. *Dev. Cell* **3**, 99–111.

Shimura H., Schlossmacher M. G., Hattori N., Frosch M. P., Trockenbacher A., Schneider R., Mizuno Y., Kosik K. S. and Selkoe D. J. (2001) Ubiquitination of a new form of alpha-synuclein by parkin from human brain: implications for Parkinson's disease. *Science* **293**, 263–269.

Sidrauski C. and Walter P. (1997) The transmembrane kinase Ire1p is a site-specific endonuclease that initiates mRNA splicing in the unfolded protein response. *Cell* **90**, 1031–1039.

Tofaris G. K., Layfield R. and Spillantini M. G. (2001) Alpha-synuclein metabolism and aggregation is linked to ubiquitin-independent degradation by the proteasome. *FEBS Lett.* **509**, 22–26.

Travers K. J., Patil C. K., Wodicka L., Lockhart D. J., Weissman J. S. and Walter P. (2000) Functional and genomic analyses reveal an essential coordination between the unfolded protein response and ER-associated degradation. *Cell* **101**, 249–258.

Trojanowski J. Q., Goedert M., Iwatsubo T. and Lee V. M. (1998) Fatal attractions: abnormal protein aggregation and neuron death in Parkinson's disease and Lewy body dementia. *Cell Death Differ.* **5**, 832–837.

Von Coelln R., Thomas B., Savitt J. M., Lim K. L., Sasaki M., Hess E. J., Dawson V. L. and Dawson T. M. (2004) Loss of locus coeruleus neurons and reduced startle in parkin null mice. *Proc. Natl Acad. Sci. U S A* **101**, 10 744–10 749.

Yang Y., Nishimura I., Imai Y., Takahashi R. and Lu B. (2003) Parkin suppresses dopaminergic neuron-selective neurotoxicity induced by Pael-R. in Drosophila. *Neuron* **37**, 911–924.

Ye J., Rawson R. B., Komuro R., Chen X., Dave U. P., Prywes R., Brown M. S. and Goldstein J. L. (2000) ER stress induces cleavage of membrane-bound ATF6 by the same proteases that process SREBPs. *Mol. Cell* **6**, 1355–1364.

Yoshida H., Matsui T., Yamamoto A., Okada T. and Mori K. (2001) XBP1 mRNA is induced by ATF6 and spliced by IRE1 in response to ER stress to produce a highly active transcription factor. *Cell* **107**, 881–891.

Zheng N., Wang P., Jeffrey P. D. and Pavletich N. P. (2000) Structure of a c-Cbl-UbcH7 complex: RING domain function in ubiquitin-protein ligases. *Cell* **102**, 533–539.

ELSEVIER

Journal of the Neurological Sciences 251 (2006) 129–133

Journal of the Neurological Sciences

www.elsevier.com/locate/jns

Short communication

Heterogeneous epileptogenicity and cortical function within malformations of cortical development: A case report

Masako Kinoshita [a], Akio Ikeda [a,*], Junya Taki [b], Keiko Usui [c], Riki Matsumoto [a], Nobuhiro Mikuni [b], Jun B. Takahashi [b], Hidenao Fukuyama [c], Nobuo Hashimoto [b], Ryosuke Takahashi [a]

[a] *Department of Neurology, Graduate School of Medicine, Kyoto University, 54 Shogoin-Kawaharacho, Sakyoku, Kyoto, 606-8507, Japan*
[b] *Department of Neurosurgery, Graduate School of Medicine, Kyoto University, 54 Shogoin-Kawaharacho, Sakyoku, Kyoto, 606-8507, Japan*
[c] *Human Brain Research Center, Graduate School of Medicine, Kyoto University, 54 Shogoin-Kawaharacho, Sakyoku, Kyoto, 606-8507, Japan*

Received 30 December 2005; received in revised form 19 July 2006; accepted 11 September 2006
Available online 13 November 2006

Abstract

The authors report a 24-year-old patient with intractable partial epilepsy and massive malformations of cortical development (MCD). Subdural EEG recordings of habitual seizures showed heterogeneous epileptogenicity, and visual evoked potential was recorded within the MCD just adjacent to the most active epileptogenic focus. Resection of the small cortical area presumably with core epileptogenicity, while sparing the cortical functional area, improved seizure outcome without any postoperative functional deficits.

Keywords: Epileptogenicity; Cortical function; Malformations of cortical development; Visual evoked potential; Subdural EEG record; Epilepsy surgery

1. Introduction

Malformations of cortical development (MCDs) are present in 15–20% of adult patients with intractable partial epilepsy [1]. However, epileptogenicity within MCD varies within as well as among individuals: epileptic activities correlate with in situ histopathologic patterns in MCD [2]. Several case reports have suggested a possibility that partial resection of MCD can give a good seizure outcome [3,4] although generally the best seizure control has been achieved when complete or major excision of both the MRI-visible lesion and the cortical areas generating ictal electrographic activity [4,5]. Recent case reports and imaging studies have shown that cortices showing MCD have normal brain functions [6–9], and therefore, resection of MCD may carry a potential risk of neurological functional deficits.

Corresponding author. Tel.: +81 75 751 3772; fax: +81 75 751 9416.
E-mail address: akio@kuhp.kyoto-u.ac.jp (A. Ikeda).

0022-510X/$ - see front matter © 2006 Elsevier B.V. All rights reserved.
doi:10.1016/j.jns.2006.09.016

Here we report a patient with partial seizures caused by MCD which had heterogeneous epileptogenicity and visual function delineated by presurgical evaluation using subdural electrodes. The most active epileptogenic area and visual functional area resided side by side within MCD. After resection of the small area of the most active epileptogenicity, the seizures significantly decreased with no functional deficits in spite of large residual MCD.

2. Patient and methods

2.1. Case presentation

A 24-year-old right-handed woman with medically intractable partial seizures had implanted subdural electrodes for presurgical evaluation. All the clinical procedures were done after full explanation about the methods and possible side effects to the patient and her family, according to clinical research protocol approved by the Ethical Committee of

Kyoto University Graduate School of Medicine (No. 79). She developed complex partial seizures (CPSs) when she was 17 years old. Her habitual seizures started with auras consisting of a sensation that something was rising from her feet and/or auditory hallucination of high-pitched sound, developed to CPSs with oral (chewing) and bilateral hand automatisms, followed by postictal cough. She had no personal or familial antecedents for epilepsy. Neurological examination showed left lower homonymous quadrianopsia. Her seizures were intractable in spite of administration of multiple drugs such as phenytoin, carbamazepine, phenobal and clobazam of appropriate dose.

An MRI revealed massive MCDs including schizencephaly and polymicrogyria in the right temporo-parieto-occipital area (Fig. 1A-D). By non-invasive video-EEG monitoring during habitual seizures consisted of motion arrest, staring, oral and hand automatisms, ictal discharges started with low-voltage fast activities at the right posterior temporal area before the clinical onset. Interictal FDG-PET showed heterogeneous regional glucose hypometabolism in the right temporo-occipital area (Fig. 1E), and ictal SPECT showed an increased perfusion in that area (Fig. 1F). Intracarotid propofol test [10] revealed language and memory dominance in the left hemisphere.

2.2. Presurgical evaluation with subdural electrodes

The electrodes were disks of 3.0 mm diameter made of platinum–iridium (Ad-Tech, Racine, WI, U.S.A.), placed with center-to-center distance of 1 cm within the silicon rubber sheet. Two sheets of 4×5 subdural electrode grid, one each on the right parietal and temporal lobes, and one 1×4 subdural electrode strip on the right temporal lobe were implanted. One set of depth electrodes made of platinum, 1.5 mm diameter, 4-contact of 1.0 mm length, with 5 mm spacing (UNIQUE MEDICAL, Tokyo, Japan), was inserted into the right antero-temporal area. The epileptogenic area was determined by simultaneous monitoring of video and subdural EEG during the patient's habitual clinical seizures.

Functional mapping was performed with the left median and tibial somatosensory evoked potential (SEP), auditory evoked potential (AEP) and visual evoked potential (VEP)

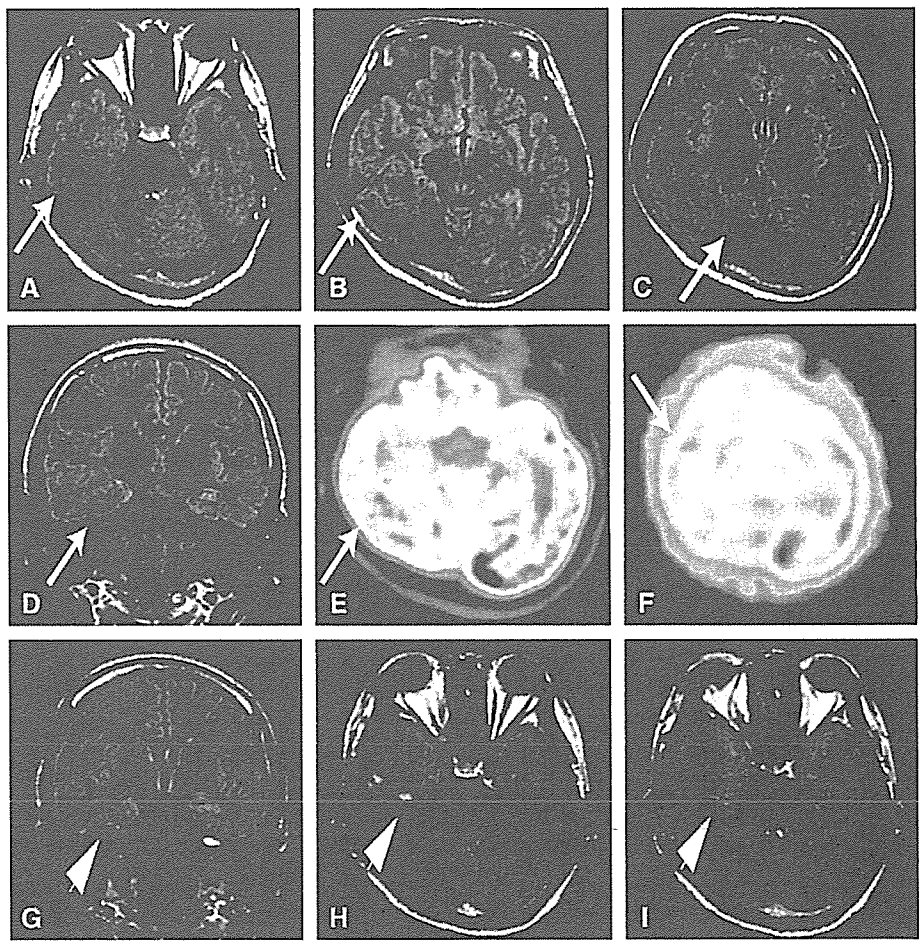

Fig. 1. Preoperative brain MRI (A–D), interictal FDG-PET (E), ictal SPECT (F) and postoperative brain MRI (G–I). (A–D) Massive MCD including a schizencephaly and polymicrogyria in the right temporo-parieto-occipital area (arrows). (E) Heterogeneous regional glucose hypometabolism in the right temporo-occipital area. (F) Ictal SPECT showed an increased perfusion in that area. (G–I) Small area with the most active epileptogenicity was resected (arrowhead). The patient showed reduction of seizures (Engel's class IIA) in spite of a large residual lesion.

studies and electric cortical stimulation. Electric cortical stimulation was performed using 50 Hz, bipolar, alternating square pulse of 0.3 ms duration.

3. Results

3.1. Delineation of epileptogenic area

She had five CPSs during the invasive monitoring period, and none of them were preceded by her typical aura. Subdural EEG showed that three seizures started with low-voltage fast activities in the posterior part of the right mesial temporal area (bold circles, Fig. 2A) followed by burst of spikes, and then spread to the lateral part. Clinical manifestation of one of them consisted of motion arrest followed by oral and bilateral hand automatisms, and the other two showed motion arrest only. One seizure with motion arrest started with low-voltage fast activities at one electrode (C4, shaded circle in Fig. 2A) in the anterior lateral temporal area, spread to basal temporal area showing rhythmic spikes. The other seizure with motion arrest and oral and bilateral hand automatisms started with spikes in the posterior part of the right lateral electrodes (A6 and A11, oblique lines in Fig. 2A). Additionally she had two habitual auras during invasive monitoring, but no EEG changes occurred. Interictal spikes were frequently seen in the mesial side of the posterior basal temporal area, and quickly spread to the adjacent electrodes (Fig. 2B and C).

3.2. Functional mapping

Pattern-reversal, visual stimulation of the fovea (3° × 3°) and central visual field (10° × 10°) evoked responses in the basal temporal area adjacent to the most active epileptogenic focus (Fig. 3). Left peripheral hemifield stimulation elicited evoked potentials in the more mesial area, while no responses were seen to the right peripheral hemifield stimulation. Median and tibial SEP and AEP showed non-primary responses at the electrodes located on the lateral superior temporal areas. Electric cortical stimulation at the basal temporal electrodes in the vicinity of the area where VEP was evoked elicited elementary and complex hallucinations in the left upper visual field in the absence of afterdischarges or her habitual auras (Fig. 4).

3.3. Surgical outcome and seizure control

The most active epileptic region in the right mesial basal temporal area within the MCD was resected tailored by

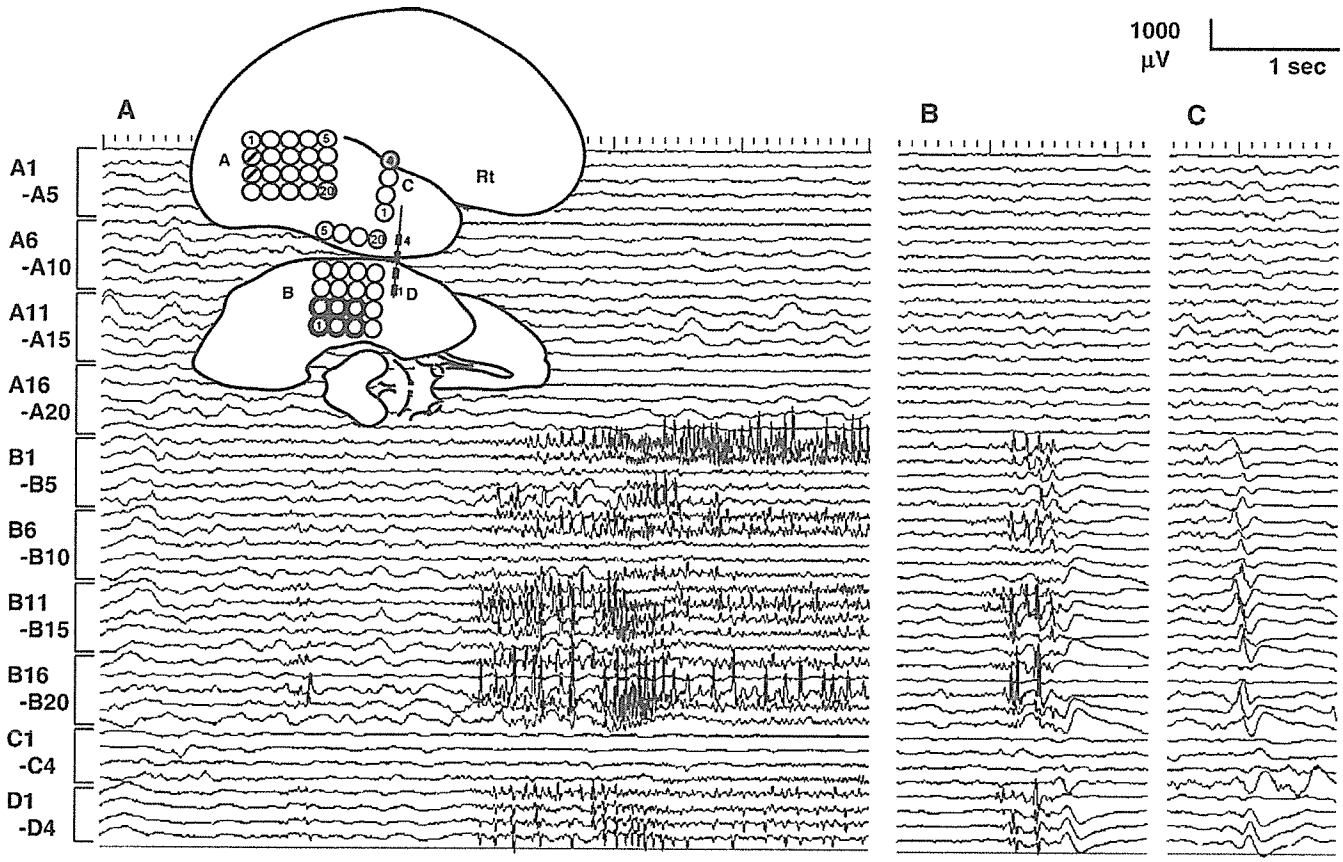

Fig. 2. Invasive EEG records. (A) Recording of a habitual seizure. Electrographic seizures most frequently started from the posterior part of the right mesial temporal area (bold circles, subdural record) approximately 15 s before the clinical onset; these areas were resected. A shaded circle and circles with oblique lines indicate other epileptogenic foci with lesser activity. (B, C) Interictal record. Interictal spikes were frequently seen in the mesial side of the posterior basal temporal area, and easily spread to the adjacent electrodes.

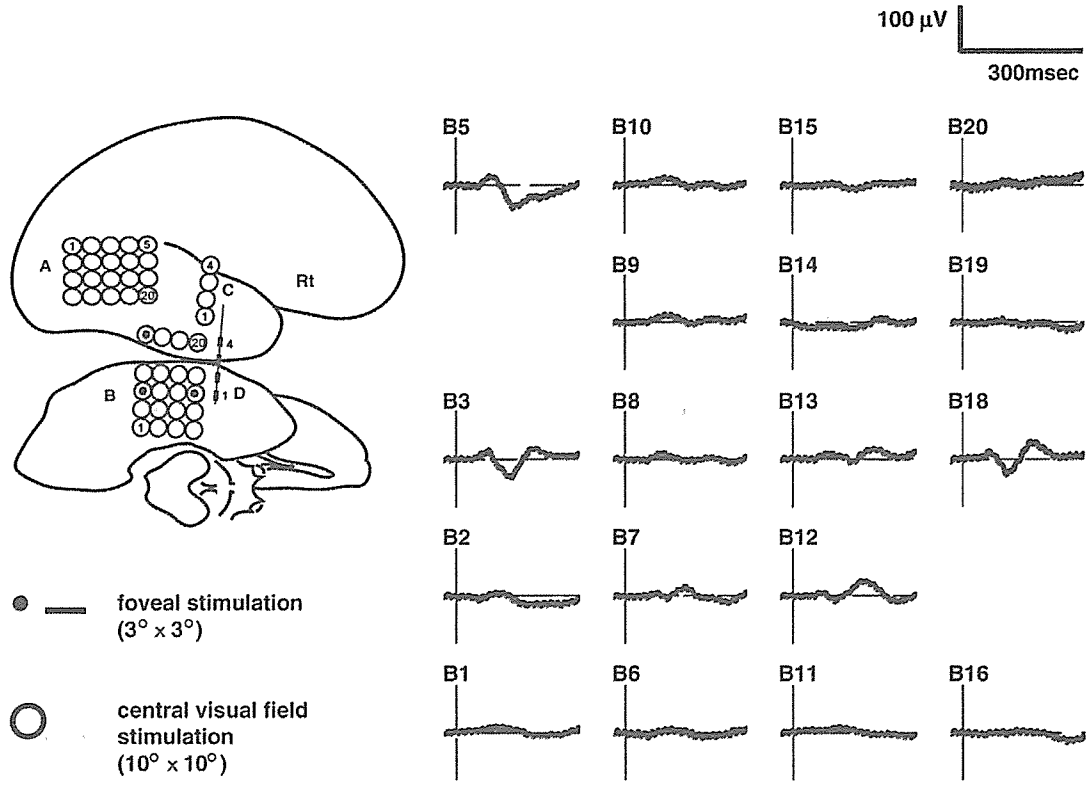

Fig. 3. VEP recording in the right basal temporal area (B plate). Foveal (dots, thick lines) and central visual field stimulation (shaded circles, gray lines) elicited responses adjacent to the most active epileptogenic area. Epilepsy surgery was performed with the best effort to spare the functional area as much as possible.

invasive EEG using subdural and depth electrodes (Figs. 1G–I and 2A) with the best effort to spare the functional area as much as possible. Histological diagnosis of the resected epileptogenic area of the patient was type IA cortical dysplasia without any balloon cells (BCs). The patient developed no neurological deficits after resection. During

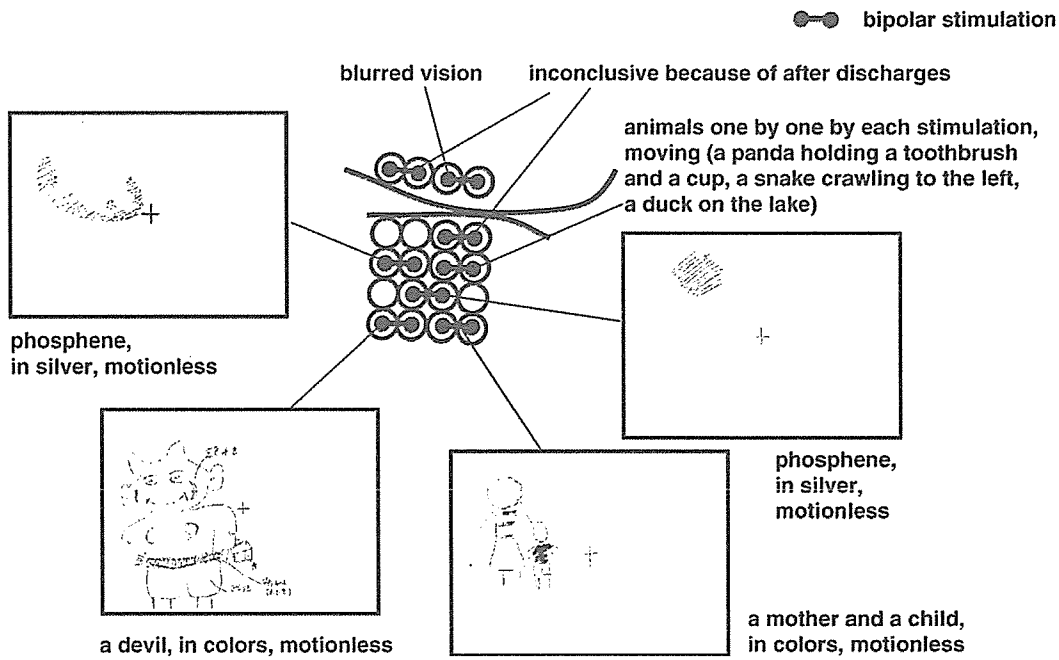

Fig. 4. Electric cortical stimulation at the basal temporal electrodes in the vicinity of the area where VEP was evoked (B plate, see Fig. 3). Elementary and complex hallucinations were elicited in the left upper visual field. Reproducibility of the symptoms was confirmed in the absence of afterdischarges or auras (insets are patient's own drawings of what she saw during stimulation).

two months after surgery the patient developed non-epileptic auditory hallucination consisting of the feeling that somebody was always talking to and chasing her, and they were totally different from her habitual auras. Before surgery, the patient had experienced the similar symptom only twice. This psychotic event was successfully controlled by neuroleptic medication of risperidone and olanzapine, therefore we consider it as post operative psychosis associated with forced normalization [11]. After a follow-up period of 2 years, the patient was in Engel's class IIA.

4. Discussion

This case demonstrated the presence of heterogeneous epileptogenicity within MCD by means of invasive EEG recording. Invasive EEG findings during habitual seizures and of interictal period suggested multiple foci within the lesion, and the most active epileptogenic region was found in the mesial side of the right basal temporal area, whose histopathology showed a mild cortical dysplasia without any BCs. The present finding is in accordance with a previous report which demonstrated, within individual MCD, that dysplastic lesions containing BCs (type IIB) were less epileptogenic than those without BCs (type I and type IIA) [2].

VEP in the present patient demonstrated that the MCD lesion in the basal temporal area participated in visual processing. In this patient, high-amplitude cortical potentials were elicited by central, foveal and left peripheral hemifield stimulation but not by right peripheral hemifield stimulation, suggesting that this cortical area possessed the function of the primary visual cortex. However, the broad distribution of VEP with the most prominent potentials in the mesial part of basal temporal area differed from the well-known, strict localization of high-amplitude responses [12]. This difference is possibly explained by atypical organization of cortical function in the present patient, as shown in previous PET and functional MRI studies [6,7]. Moreover, this patient showed elementary and complex visual hallucinations when the basal temporal area was stimulated. Elementary hallucinations occur with the involvement of the primary visual cortex [13], and thus if they were observed during spontaneous temporal lobe seizures or upon electrical stimulation of the temporal lobe, usually they were explained by the spread of activity to the occipital lobe [13]. Therefore, elementary hallucinations in this patient produced by electric stimulation suggest the atypical location of the primary visual cortex in the basal temporal area.

In summary, this case report demonstrated that the seizure reduction with sparing the functional area can be achieved by precise presurgical evaluation using subdural electrodes, including electric cortical stimulation, recordings of habitual seizures and evoked potentials. More case accumulation is warranted to prove the notion that it is possible to achieve not only the maximum seizure reduction but also the minimum functional deficits by epilepsy surgery.

Acknowledgment

The authors thank Dr. Akira Sengoku, Sengoku clinic, Kyoto-shi, Japan, for referring the patient. This study was supported by the Research Grant for the Treatment of Intractable Epilepsy (16-1) from the Japan Ministry of Health, Labour and Welfare, and Scientific Research Grant (C2) from the Japan Society for Promotion of Science (JSPS).

References

[1] Kuzniecky RI, Jackson GD. Developmental disorders. In: Engel Jr J, Pedley TA, editors. Epilepsy A Comprehensive Textbook. Philadelphia: Lippincott-Raven; 1997, p. 2517–32.
[2] Boonyapisit K, Najm I, Klem G, Ying Z, Burrier C, LaPresto E, et al. Epileptogenicity of focal cortical malformations due to abnormal cortical development: direct electrocorticographic–histopathologic correlations. Epilepsia 2003;44(1):69–76.
[3] Francione S, Vigliano P, Tassi L, Cardinale F, Mai R, Lo Russo G, et al. Surgery for drug resistant partial epilepsy in children with focal cortical dysplasia: anatomical–clinical correlations and neurophysiological data in 10 patients. J Neurol Neurosurg Psychiatry 2003;74:1493–501.
[4] Chassoux F, Devaux B, Landré E, Turak B, Nataf F, Varlet P, et al. Stereoelectroencephalography in focal cortical dysplasia. A 3D approach to delineating the dysplastic cortex. Brain 2000;123:1733–51.
[5] Palmini A, Gambardella A, Andermann F, Dubeau F, da Costa JC, Olivier A, et al. Operative strategies for patients with cortical dysplastic lesions and intractable epilepsy. Epilepsia 1994;35:S57–71.
[6] Janszky J, Ebner A, Kruse B, Mertens M, Jokeit H, Seitz RJ, et al. Functional organization of the brain with malformations of cortical development. Ann Neurol 2003;53:759–67.
[7] Richardson MP, Koepp MJ, Brooks DJ, Coull JT, Grasby P, Fish DR, et al. Cerebral activation in malformations of cortical development. Brain 1998;121:1295–304.
[8] Innocenti GM, Maeder P, Knyazeva MG, Fornari E, Deonna T. Functional activation of microgyric visual cortex in a human. Ann Neurol 2001;50:672–6.
[9] Mikuni N, Ikeda A, Yoneko H, Amano S, Hanakawa T, Fukuyama H, et al. Surgical resection of an epileptogenic cortical dysplasia in the deep foot sensorimotor area. Epilepsy Behav 2005;7:559–62.
[10] Takayama M, Miyamoto S, Ikeda A, Mikuni N, Takahashi JB, Usui K, et al. Intracarotid propofol test for speech and memory dominance in man. Neurology 2004;63:510–5.
[11] Andermann LF, Savard G, Meencke HJ, McLachlan R, Moshe S, Andermann F. Psychosis after resection of ganglioglioma or DNET: evidence for an association. Epilepsia 1999;40:83–7.
[12] Noachtar S, Hashimoto T, Lüders H. Pattern visual evoked potentials recorded from human occipital cortex with chronic subdual electrodes. Electroencephalogr Clin Neurophysiol 1993;88:435–46.
[13] Bien CG, Benninger FO, Urbach H, Schramm J, Kurthen M, Elger CE. Localizing value of epileptic visual auras. Brain 2000;123:244–53.

Journal of Neuroscience Research 85:153–165 (2007)

Presenilin 1 Is Involved in the Maturation of β-Site Amyloid Precursor Protein-Cleaving Enzyme 1 (BACE1)

Akira Kuzuya,[1] Kengo Uemura,[1] Naoyuki Kitagawa,[1] Nobuhisa Aoyagi,[1] Takeshi Kihara,[2] Haruaki Ninomiya,[3] Shoichi Ishiura,[4] Ryosuke Takahashi,[1] and Shun Shimohama[1]*

[1]Department of Neurology, Graduate School of Medicine, Kyoto University, Kyoto, Japan
[2]Department of Neuroscience for Drug Discovery, Graduate School of Pharmaceutical Sciences, Kyoto University, Kyoto, Japan
[3]Department of Neurobiology, Tottori University, Faculty of Medicine, Yonago, Japan
[4]Department of Life Sciences, Graduate School of Arts and Sciences, University of Tokyo, Tokyo, Japan

One of the pathologic hallmarks of Alzheimer's disease is the excessive deposition of β-amyloid peptides (Aβ) in senile plaques. Aβ is generated when β-amyloid precursor protein (APP) is cleaved sequentially by β-secretase, identified as β-site APP-cleaving enzyme 1 (BACE1), and γ-secretase, a putative enzymatic complex containing presenilin 1 (PS1). However, functional interaction between PS1 and BACE1 has never been known. In addition to this classical role in the generation of Aβ peptides, it has also been proposed that PS1 affects the intracellular trafficking and maturation of selected membrane proteins. We show that the levels of exogenous and endogenous mature BACE1 expressed in presenilin-deficient mouse embryonic fibroblasts (PS−/−MEFs) were reduced significantly compared to those in wild-type MEFs. Moreover, the levels of mature BACE1 were increased in human neuroblastoma cell line, SH-SY5Y, stably expressing wild-type PS1, compared to native cells. Conversely, the maturation of BACE1 was compromised under the stable expression of dominant-negative mutant PS1 overexpression. Immunoprecipitation assay showed that PS1 preferably interacts with proBACE1 rather than mature BACE1, indicating that PS1 can be directly involved in the maturation process of BACE1. Further, endogenous PS1 was immunoprecipitated with endogenous BACE1 in SH-SY5Y cells and mouse brain tissue. We conclude that PS1 is directly involved in the maturation of BACE1, thus possibly functioning as a regulator of both β- and γ-secretase in Aβ generation.

Key words: Alzheimer's disease; amyloid; γ-secretase; β-secretase

Alzheimer's disease (AD) is pathologically characterized by the excessive accumulation and deposition of β-amyloid peptides (Aβ) (Kang et al., 1987). Because the longer Aβ peptide species, Aβ1-42 (Aβ42), aggregates more readily than the shorter and more predominant species, Aβ1-40 (Aβ40), it is believed that Aβ42 plays an important role in AD pathogenesis (Hardy, 1997a,b). Aβ peptides are generated by the consecutive proteolysis of β-amyloid precursor protein (APP), by distinct enzymatic moieties known as β-secretase and γ-secretase (Golde et al., 1993; Haass et al., 1993). Recently, primary β-secretase in the brain was identified as a membrane-associated aspartyl protease, β-site APP-cleaving enzyme 1 (BACE1) (Hussain et al., 1999; Sinha et al., 1999; Vassar et al., 1999; Yan et al., 1999; Haniu et al., 2000). BACE1 generates a membrane-bound APP C-terminal fragment (APP CTFβ), which undergoes intra-membranous γ-secretase cleavage to generate the Aβ peptide. Although multiple lines of biochemical and genetic evidence have shown that γ-secretase forms high molecular weight complexes containing at least presenilin 1 (PS1), nicastrin, aph-1, and pen-2 (Capell et al., 1998; Yu et al., 2000; Edbauer et al., 2002; Francis et al., 2002; Lee et al., 2002; Steiner et al., 2002; Gu et al., 2003), the functional interaction of β- and γ-secretase in Aβ generation still remains unclear.

Importantly, mutations in PS1 are the most common known cause of autosomal dominant familial Alzheimer's disease (FAD) (Rogaev et al., 1995; Sherrington et al., 1995; Thinakaran 1999). These mutations increase the level of Aβ42/40 in transfected mammalian cells and the

Contract grant sponsor: Ministry of Education, Culture, Sports, Science and Technology of Japan; Contract grant sponsor: Japan Society for the Promotion of Science; Contract grant sponsor: Ministry of Health, Labour and Welfare of Japan; Contract grant sponsor: Smoking Research Foundation; Contract grant sponsor: Philip Morris USA, Inc.; Contract grant sponsor: Philip Morris International.

*Correspondence to: Dr. Shimohama, Department of Neurology, Graduate School of Medicine, Kyoto University, 54 Shogoin-Kawaharacho, Sakyo-ku, Kyoto 606-8507, Japan.
E-mail: i53367@sakura.kudpc.kyoto-u.ac.jp

Received 20 January 2006; Revised 25 May 2006; Accepted 4 September 2006

Published online 30 October 2006 in Wiley InterScience (www.interscience.wiley.com). DOI: 10.1002/jnr.21104

brains of transgenic mice (Borchelt et al., 1996; Duff et al., 1996). Whereas it has generally been accepted that PS1 is the essential catalytic component of γ-secretase (Wolfe et al., 1999a,b), it has also been reported that Aβ is still generated in absence of both PS1 and its homologue PS2 (Armogida et al., 2001; Wilson et al., 2002). In addition, it has also been proposed that PS1 affects the intracellular trafficking and maturation of selected membrane proteins. Indeed, PS1 deficiency affects the intracellular trafficking and maturation of TrkB, as well as ICAM5/telenchephalin in neurons (Naruse et al., 1998; Annaert et al., 2001). We have also shown that PS1 regulates the intracellular trafficking and maturation of N-cadherin in SH-SY5Y cells (Uemura et al., 2003a). Furthermore, it has been shown that PS1 is involved in regulating the intracellular trafficking and maturation of APP and nicastrin, which are essential for Aβ generation (Kim et al., 2001; Edbauer et al., 2002; Leem et al., 2002a,b; Cai et al., 2003; Herreman et al., 2003). Although there is no reported genetic linkage between mutations in BACE1 and AD to date, recent reports have shown an elevation of BACE1 protein expression and its enzymatic activity in AD brains (Fukumoto et al., 2002; Holsinger et al., 2002; Yang et al., 2003), indicating that BACE1, as well as PS1, is involved significantly in AD pathogenesis. Recently, Kamal et al. (2001) showed that APP, PS1, and BACE1 are transported in the same membrane vesicles along the axons in vivo, via the direct binding of APP to the kinesin light chain subunit of kinesin-I, a microtubule motor protein. These observations raise the possibility that PS1 is related functionally to the intracellular trafficking and maturation of BACE1 through the amyloidogenic pathway of APP.

Based on the above observations, we hypothesized that PS1 influences the intracellular trafficking and maturation of BACE1. To characterize the effect of PS1 on the trafficking-dependent maturation of BACE1, wild-type (wt) and presenilin-deficient mouse embryonic fibroblast cell lines (MEFs) or human neuroblastoma SH-SY5Y cell lines stably expressing either wt PS1 or dominant-negative PS1 were used in the present study. We report that wt PS1 binds BACE1 directly and upregulates its maturation, whereas the absence of PS1 or dominant-negative PS1 downregulates its maturation. Taking the previous reports and our results together, we suggest that PS1 significantly modulates both β- and γ-secretase via regulation of the intracellular trafficking of both secretase, and operates as a primary regulator determining the amyloidogenic processing of APP.

MATERIALS AND METHODS

Cell Cultures, Constructs, Transfection and Brain Tissue

The generation of SH-SY5Y cells stably expressing either wild-type PS1 (wt PS1) or dominant-negative (D385A) PS1 has been described previously (Uemura et al., 2003b). In the present experiments, we used native SH-SY5Y cells as control cells. Wild-type (wt) and PS1/PS2 (PS−/−) double knockout mouse embryonic fibroblast (MEF) cell lines (Herreman et al., 1999, 2003) were kindly provided by Dr. De Strooper (Center for Human Genetics, KUL, VIB, Belgium). These cell lines were maintained in Dulbecco's modified Eagle's medium (DMEM; Nissui Pharmaceutical, Tokyo, Japan) containing 10% fetal bovine serum (FBS), 100 IU/ml penicillin, 100 μg/ml streptomycin and glutamine (2 mM) (Life Technologies, Rockville, MD) at 37°C in 5% CO_2. Stably transfected SH-SY5Y cells were selected and maintained with 300 mg/ml G418 (Wako Pure Chemical Industries, Ltd., Osaka, Japan). For immunoprecipitation experiment using the SH-SY5Y cell lines, the cells were cultured in Opti-MEM I (Gibco BRL, Rockville, MD) containing 10% FBS to grow at full confluency. An expression vector to encode HA-tagged human full-length BACE1 has been described previously (Hattori et al., 2002). An expression vector to encode FAD-linked PS1 mutant containing proline (Pro) to leucine mutation at position Pro-117 (P117L PS1) has been described previously (Uemura et al., 2003b). An expression vector to encode GFP was purchased from Invitrogen. Lipofectamine 2000 (Invitrogen Life Technologies) was used for transient cotransfection of BACE1 and GFP constructs into MEF cells, according to the instruction. During and after the transfection, cells were maintained in Opti-MEM I. GFP was cotransfected with BACE1, using as an indicator of transfection efficiency. To obtain comparable expression levels of GFP between wt and PS−/− MEF cells, the transfection condition was optimized by varying doses of DNA and Lipofectamine 2000. Rat primary cultures were obtained from the fetal rat cerebral cortex (17–19 days gestation) and were maintained as described previously (Kihara et al., 1997). Mouse primary cultures were prepared as described previously (Uemura et al., 2006). Only mature neurons were used for the present experiments. For the treatment of γ-secretase inhibitors to primary cultures, the medium containing either 2 μM L-685,458 or 1 μM DAPT were exchanged every day for 4 days. Control cells were treated with vehicle (DMSO) only. Fresh brain tissue was prepared from 3-month-old mice. The animals were treated in accordance with the guidelines published in the National Institutes of Health Guide for the Care and Use of Laboratory Animals.

Antibodies and Reagents

Monoclonal antibody MAB5308 against the C terminus of BACE1, monoclonal antibody MAB5232 against the loop domain of PS1 and rabbit polyclonal anti-mannosidase II antibody were purchased from Chemicon (Temecula, CA). Monoclonal and rabbit polyclonal anti-HA antibodies, monoclonal anti-β-actin antibody, rabbit polyclonal anti-APP antibody recognizing the C terminus and rabbit polyclonal anti-BACE1 antibody, EE-17, recognizing the N terminus (amino acids 46–62), were purchased from Sigma (St. Louis, MO). Rabbit polyclonal anti-proBACE1 antibody (targeting amino acids 26–45 corresponding to the prodomain sequence), rabbit polyclonal anti-BACE1 antibody (targeting amino acids 485–501) and rabbit polyclonal anti-BACE1 antibody (targeting amino acids 487–501) were purchased from Calbiochem. Rabbit polyclonal anti-calnexin antibody was purchased from StressGen (Victoria, BC). Rabbit polyclonal anti-PS1 antibody against the N terminus was purchased from Santa Cruz Biotechnology (Santa Cruz, CA). Rabbit polyclonal anti-GFP antibody was purchased from

TABLE I. Antibodies used in Experiment

Antigen	Name	Epitope	Host
BACE1	MAB5308	C-terminus	Monoclonal
	Anti-BACE1	C-terminus (aa 487–501)	Polyclonal rabbit
	Anti-BACE1	C-terminus (aa 485–501)	Polyclonal rabbit
	EE-17	N-terminus (aa 46–62)	Polyclonal rabbit
	Anti-proBACE1	Prodomain (aa 26–45)	Polyclonal rabbit
PS1	Anti-PS1	N-terminus	Polyclonal rabbit
	MAB5232	Loop domain	Monoclonal

Molecular Probes (Eugene, OR). For immunostaining, Alexa Fluor 546 goat anti-mouse IgG (H+L) conjugate and Alexa Fluor 488 goat anti-rabbit IgG (H+L) conjugate (Molecular Probes) were used as secondary antibodies. In Table I, the corresponding epitopes of anti-PS1 and anti-BACE1 antibodies used in the present experiment are summarized. Two well-characterized γ-secretase inhibitors, L-685,458 and *N*-[*N*-(3,5-difluorophenacetyl)-L-alanyl]-*S*-phenylglycine *t*-butyl ester (DAPT) were purchased from Sigma and Calbiochem, respectively.

Reverse Transcription-Polymerase Chain Reaction

Total RNA was extracted from confluent cells of each cell line by using ISOGEN (Nippon Gene, Toyama, Japan). Equal amounts of total RNA obtained from each cell line were processed for cDNA synthesis using oligo (dT) primers and reverse transcriptase, using a RNA LA PCR kit (AMV) (TaKaRa, Tokyo, Japan). They were amplified by polymerase chain reaction (PCR) using sense and anti-sense primers specific for either the human *BACE1* gene (5′CATTGGAGGTATCGACCACTCGCT3′ and 5′CCACAGTCTTCCATGTCCAA-GGTG3′, the product size was 624 bp; GenBank accession number AF190725) or the human *glyceraldehyde-3-phosphate dehydrogenase* (*GAPDH*) gene (5′ACCACAGTCCATGCCATCAC3′ and 5′TCCACCACCCTGTTGCTGTA3′, 452 bp; J04038). The amplification program consisted of a denaturing step at 94°C for 1 min, an annealing step at 62°C for 40 src, and an extension step at 72.9°C for 50 sec. This was repeated 25 cycles for BACE and 18 cycles for GAPDH. The PCR products separated on a 1.5% agarose gel were stained by ethidium bromide and visualized using a UV transilluminator coupled to a CCD camera.

Preparation of Protein Samples, Western Blot Analysis, and immunoprecipitation

Confluent cells were rinsed three times with ice-cold phosphate-buffered saline (PBS) and centrifuged. Each pellet was suspended in TNE buffer (10 mM Tris-Hcl, pH 7.8, 1% NP40, 0.15 M NaCl, 1 mM EDTA) supplemented with 1 mM dithiothreitol (DTT) and 1 mM phenylmethylsulphonyl fluoride (PMSF), dispersed by pipetting vigorously 20 times and then rotated for 1 hr at 4°C. Each sample was then centrifuged at 25,000 × *g* for 30 min at 4°C and the supernatants were collected to obtain the protein samples. Protein concentration was determined using the Bradford assay (Bradford, 1976). Equal amounts of protein were treated with Protein G-Sepharose (Amersham Biosciences, Uppsala, Sweden) overnight at 4°C. After removing Protein G-Sepharose by centrifugation at 2,000 × *g* for 5 min, either the MAB5308 antibody, the anti-BACE1 antibody (Calbiochem), or anti-PS1 antibody (Santa Cruz Biotechnology, Santa Cruz, CA) was added to the lysate. Each sample was rotated for 1 hr at 4°C and then treated with Protein G-Sepharose for 1 hr at 4°C. The immunoprecipitates were washed with TNE buffer five times and resuspended in 2× sample buffer (125 mM Tris-HCl [pH 6.8], 4.3% SDS, 30% glycerol, 10% 2-mercaptoethanol, and 0.01% bromophenol blue). After boiling for 3 min, the supernatants were subjected to Western blotting. For the detection of full-length PS1, the suspension was incubated at 37°C for 10 min instead of boiling. Alternatively, confluent cells were rinsed three times with ice-cold PBS and scraped off. Cell pellets were suspended in TNE buffer supplemented with 1 mM DTT and 1 mM PMSF, and sonicated. The samples were centrifuged at 25,000 × *g* for 30 min at 4°C and the supernatants were collected to obtain protein samples. Protein concentration was determined using the Bradford assay, and then equal amounts of cell extracts were subjected to Western blotting.

In Western blot analysis, samples were electrophoresed on polyacrylamide gels in the presence of SDS. Immunoblotting was carried out by transferring the proteins to polyvinylidene difluoride microporous membrane, which was then blocked with 5% skimmed milk in 10 mM PBS containing 0.1% Tween 20 (PBS-T), and incubated with the primary antibodies in PBS-T containing 4% BSA overnight at 4°C. The membranes were then washed in PBS-T and incubated with a horseradish peroxidase-conjugated anti-mouse or anti-rabbit IgG (Amersham, Little Chalfont, UK) in PBS-T for 1 hr at room temperature. The specific reaction was visualized, using the enhanced chemiluminescence method (ECL) (Amersham).

Immunostaining

Immunostaining was carried out as described previously (Uemura et al., 2003b). Briefly, SH-SY5Y cell lines and 5 days in vitro primary cultures were fixed with 4% paraformaldehyde for 20 min. Fixed cells were blocked with 3% BSA in PBS with 0.2% Triton X-100 for 15–20 min and incubated overnight at 4°C with primary antibodies diluted in PBS containing 3% BSA. Immunoreactivity was visualized using the species-specific secondary antibodies mentioned above. Samples were observed using a LSM (Zeiss) confocal scanning microscope.

Statistical Analysis

The relative density of the bands in RT-PCR or Western blot was analyzed by quantitative densitometry using a computerized image analysis program (NIH Image 1.59). To compare either the levels of mature BACE1 or the mature:proBACE1 ratio among the SH-SY5Y cell lines, statistical analysis was carried out using one-way ANOVA, followed by post-hoc Fisher's protected least significant difference. To compare the mature BACE1:GFP ratio or the mature:proBACE1 ratio between wt MEFs and PS−/− MEFs, statistical analysis was carried out using Student's *t*-test. Data were expressed as the mean ± SD, and significance was assessed at $P < 0.01$.

RESULTS

PS1 Is Involved in BACE1 Maturation

Previous studies showed that BACE1 undergoes core glycosylation in the endoplasmic reticulum (ER) cotranslationally, and is produced as proBACE1. Then, short-lived proBACE1 is transported from the ER to the Golgi apparatus, and undergoes rapid maturation by the proteolytic removal of the prodomain followed by complex *N*-glycosylation in the Golgi apparatus (Capell et al., 2000; Haniu et al., 2000; Huse et al., 2000; Creemers et al., 2001). Finally, mature BACE1 is quite stable unlike proBACE1, and is located in the late secretory compartments, the plasma membrane, and the endosomal compartments (Huse et al., 2000; Walter et al., 2001).

To examine a possible role for PS1 in regulating BACE1 maturation, we first investigated the effect of PS deficiency on BACE1 maturation, using PS1 and its homologue PS2 double-knockout (PS−/−) mouse embryonic fibroblasts (MEFs) (Herreman et al., 1999, 2003). HA-tagged wt BACE1 and GFP plasmids were transiently cotransfected into wt and PS−/− MEFs, and the cells were collected 24 hr after transfection. Each cell lysate was subjected to Western blot analysis using either monoclonal anti-HA antibody or anti-GFP antibody. As shown in Figure 1A, the immunoblotting bands of HA-tagged BACE1 were detected as two different molecular weight bands. The higher molecular weight bands represented mature BACE1, complex N-glycosylated one, whereas the lower molecular weight bands represented proBACE1, a precursor of mature BACE1 (Capell et al., 2000). Interestingly, the levels of mature BACE1 were apparently reduced in PS−/− MEFs compared to wt MEFs, whereas the levels of GFP were comparable between them, indicating that the transfection efficiency was not different (Fig. 1A). Quantitative analysis showed that the ratio of mature BACE1:GFP was reduced by 70% in PS−/− MEFs, compared to that in wt MEFs (Fig. 1B; $n = 4$, $P < 0.0005$). In addition, the ratio of mature:proBACE1 was reduced by 50% in PS−/− MEFs, compared to that in wt MEFs (Fig. 1C, $n = 4$, $P < 0.0005$). These data suggest that the expression level of PS affects significantly the maturation of BACE1 in MEF cells. To further confirm the effect of PS expression on BACE1 maturation at endogenously expressed level, we compared the levels of endogenous BACE1 between wt and PS−/− MEFs. Equal amounts of cell lysates obtained from wt and PS−/− MEFs were subjected to Western blotting, using anti-BACE1 antibody (targeting amino acid 485–501), and anti-proBACE1 antibody. Lysates of mouse brain tissue and mouse primary neurons were used as positive controls. As expectedly, the level of mature BACE1 in PS−/− MEFs was reduced drastically as compared to that in wt MEFs, whereas the levels of β actin were almost constant between them (Fig. 1D). Interestingly, we observed no significant difference in the levels of proBACE1 between them, indicating that the maturation of endogenous BACE1 was remarkably inhibited in PS−/− MEFs as compared to in wt MEFs (Fig. 1D). We then asked whether the maturation of exogenously expressed BACE1 is affected by co-expression of either wt PS1 or P117L PS1 mutant causing FAD. Plasmids to encode either GFP, wt PS1, or P117L PS1 were cotransfected with HA-tagged BACE1 plasmid into PS−/− MEFs by 1:1 ratio. The cells were collected 24 hr after transfection, and each cell lysate was subjected to Western blotting analysis using either rabbit polyclonal anti-HA antibody or anti-PS1 antibody (against the N terminus). As shown in Figure 1E, the levels of mature and proBACE1 were increased drastically in the cells expressing either wt PS1 or P117L PS1 as compared to those in the cells expressing GFP, whereas the levels of wt PS1 and P117L PS1 were almost similar. This result suggests that both wt PS1 and P117L PS1 similarly upregulate the stability of both mature and proBACE1 in this experimental system. The above data suggest that the expression level of PS is involved significantly in the stabilization and maturation of BACE1 in MEF cells.

To examine a specific role for PS1 in BACE1 maturation in neuronal cells, we used SH-SY5Y cells stably expressing either wild-type PS1 (wt PS1) or PS1 containing aspartate (Asp) to alanine mutation at position Asp-385 (D385A PS1). As described previously, exogenous overexpression of D385A PS1 that fails to undergo endoproteolysis, significantly replaces endogenous PS1 and results in a dominant negative version of PS1 in SH-SY5Y cells (Uemura et al., 2003b). To specifically identify either proBACE1 or mature BACE1, equal amounts of cell lysate obtained from each cell line were subjected to Western blotting using the anti-proBACE1 antibody (targeting amino acids 26–45 corresponding to the prodomain sequence) and the antibody EE-17 (targeting amino acids 46–62 corresponding to the neoepitope after removal of the prodomain), respectively. It has been reported that neoepitope antibodies specific for BACE1 after removal of the prodomain preferentially recognize the mature BACE1 polypeptide (Capell et al., 2000). Indeed, the antibody EE-17 detected the mature BACE1 polypeptide in a higher molecular weight band of 70–75 kDa that represented its complex *N*-glycosylation, whereas the anti-proBACE1 antibody detected the proBACE1 polypeptide in a tighter band of 65 kDa in lysates from each cell line (Fig. 2A). These results are consistent with the molecular weight of BACE1 described previously (Vassar et al., 1999; Capell et al., 2000; Pinnix et al., 2001). Quantitative analysis showed that the amount of mature BACE1 was increased by 20% in wt PS1 cells and was reduced by 50% in D385A PS1 cells, compared to that in control cells (Fig. 2B; $n = 3$, $\#P < 0.01$ vs. control, $*P < 0.0001$). Interestingly, the ratio of mature:proBACE1 was reduced significantly by 60% in D385A PS1 cells, compared to that in control cells, whereas it was not statistically different between control and wt PS1 cells (Fig. 2C; $n = 3$, $*P < 0.001$ vs. control).

To investigate whether the difference in BACE1 protein levels among these cell lines is dependent on the mRNA expression levels, the level of BACE1 mRNA expression in these cell lines was quantitated by semi-quantitative reverse transcription-polymerase chain reaction (RT-PCR) analysis. Expression of both BACE1 mRNA